



# Imaging Cardiac Metabolism

# 9

Heinrich Taegtmeyer and Vasken Dilsizian

## Introduction

*Cardiac metabolism* refers to a complex system of interconnected chemical reactions. In broad terms, metabolism provides the energy for contraction and the materials for the heart's structure and function. A defining feature of metabolism is the flux of chemical compounds that can be traced by physical methods, including radioactive decay of tracers or magnetic resonance (MR) spectroscopy. These methods are readily applied both *in vivo* and *ex vivo* for the assessment of cardiac metabolic activity [1]. Metabolic activity, in turn, is a dynamic process found only in living cells and tissues. In addition to this dynamic nature of metabolic activity, intermediary metabolites also control cell function, either as regulators of enzyme activity or as posttranslational modifiers of protein function and transcriptional activity [2, 3].

An important recent development in the field of nuclear cardiology is the concept that metabolic remodeling of the heart precedes, triggers, and sustains structural and functional remodeling, and that metabolism is inextricably linked to both physiology and molecular biology of the heart. This concept offers unprecedented opportunities for metabolic imaging [4].

The pathways of myocardial energy substrate metabolism converge on the energy-rich phosphate bonds of ATP (Fig. 9.1). ATP is largely used to maintain myocardial contraction and to regulate the membrane pumps and movements of ions in and out of the cell. For a given physiologic environment, the heart consumes the most efficient metabolic fuel for its function [6]. In the normally oxygenated heart, fatty acids account for the majority of ATP production; glucose makes only a small contribution in providing energy, unless there is an insulin surge. During an acute increase in work load (for example, inotropic stimulation), the heart immediately mobilizes its metabolic reserve contained in glycogen (transient increase in glycogen oxidation) and meets the needs for additional energy from the oxidation of carbohydrate substrates (glucose and lactate). When the oxygen supply is decreased, the heart protects itself from an oxygen-deficient state by switching its energy source to glycolysis, downregulating mitochondrial oxidative metabolism and reducing contractile function. Thus, the tight coupling between metabolism and contractile function in the heart offers a unique opportunity to assess cardiac performance in coronary flow, myocardial perfusion, oxygen delivery, metabolism, and contraction.

The advantages of imaging cardiac metabolism rest in the observer's ability to monitor and trace chemical processes in the heart by noninvasive methods. In reality, cardiac metabolism consists of a complex and highly regulated biological network of intracellular reactions that is well characterized at the biochemical level [1].

---

H. Taegtmeyer (✉)  
The University of Texas Health Science Center at Houston,  
McGovern Medical School, Houston, TX, USA  
e-mail: [Heinrich.Taegtmeyer@uth.tmc.edu](mailto:Heinrich.Taegtmeyer@uth.tmc.edu)

V. Dilsizian  
University of Maryland School of Medicine, Baltimore, MD, USA

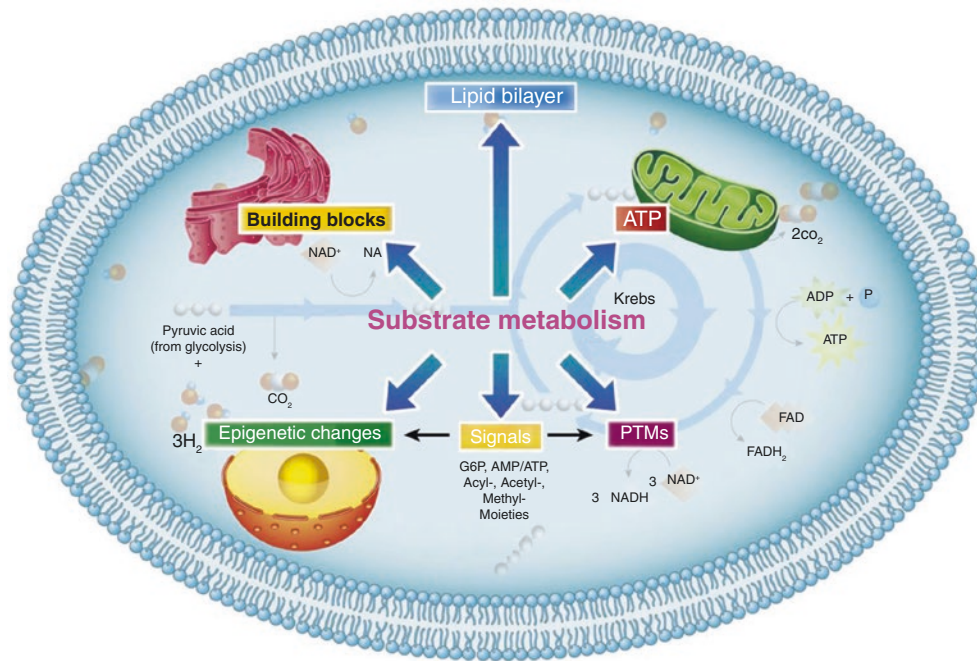


**Fig. 9.1** Multiple roles of metabolism. Products of energy substrate metabolism provide ATP, building blocks of complex molecules, including proteins and ribonucleotides, as well as lipid bilayers, substrates for posttranslational modifications of proteins (PTMs), and metabolic signals such as glucose 6-phosphate (G6P), the AMP/ATP ratio,

and acyl-, acetyl-, and methyl- groups serving as substrates for epigenetic changes or for PTMs. This drawing attempts to show the main features of metabolism in the heart. (From Davogustto and Taegtmeier [5]; with permission from Elsevier)

No doubt, the interrelationship between mechanical function, myocardial perfusion, and metabolic and energy-consuming processes within the heart is complex. Existing knowledge can be reduced to a few principles: A metabolic switch from fatty acids to glucose seems pivotal in preserving myocardial viability and likely represents the earliest adaptive response to myocardial ischemia. Perhaps the most dramatic clinical application for the metabolic switch from fatty acid utilization to glycolysis is in myocardial hibernation. Hibernating myocardium represents the dysfunctional but viable myocardium, most likely the result of extensive cellular reprogramming due to repetitive episodes of chronic ischemia. This reprogramming of myocytes occurs at multiple levels. Although the true mechanism for viability remodeling in hibernation is likely to be very complex, it is thought to be related, in part, to the increased glycogen content and myocardial ATP levels in such cells, simulating the fetal heart. Because glucose transport and phosphorylation is readily traced by the uptake and retention of  $^{18}\text{F}$ -fluoro,2-deoxy-D-glucose (FDG), hibernating myocardium is readily detected by enhanced glucose uptake in the same regions by external detectors, such as positron emission tomography (PET).

Recent clinical studies have also shown the potential utility of metabolic adaptation in the emergency department as well as for detection of coronary artery disease in the form of “ischemic memory.” Ischemic memory represents prolonged but reversible metabolic recovery after transient myocardial ischemia, also known as “metabolic stunning.” At the cellular level, it is the result of extensive transcriptional, translational, and post-translational metabolic changes.

Other disease entities in which metabolic imaging by nuclear techniques can play an important role include diabetic heart disease, the identification of microvascular disease and subendocardial ischemia in symptomatic patients with nonobstructive coronary artery disease, and left ventricular remodeling in hypertrophy and congestive heart failure. The understanding of this kind of left ventricular remodeling has increased dramatically in recent years. Emerging evidence suggests a role for altered metabolism in the progression of both left ventricular hypertrophy and remodeling. Some of the clinical evidence includes a variable prognosis in patients with similar left ventricular mass in hypertrophy; a loss of metabolic flexibility that may portend worse prognosis in patients with heart failure; and the development of modulators for medical treatment in heart failure, such as fatty acid oxidation inhibitors (e.g., ranolazine) and insulin sensitizers.

Metabolic adaptation serves as a mechanism of cell survival in response to an altered physiological state and represents one of the earliest responses to myocardial ischemia, left ventricular remodeling, and diabetic and uremic heart disease. Recognizing key intracellular signals that link energy substrate metabolism with gene expression may allow the discovery of more specific molecular targets for the imaging, diagnosis, and treatment of cardiovascular disease.

## Evolution of Knowledge of Cardiac Metabolism

The acquisition of knowledge of cardiac metabolism is highlighted by a number of early milestones:

- *1854*: Hermann von Helmholtz discovers the first law of thermodynamics, introducing the concept that energy bound up in foodstuffs is liberated and transferred to physical work.
- *1857*: Louis Pasteur discovers that fermentation occurs in living microorganisms and can be turned off by oxygen. When the oxygen supply is diminished, the rate of glucose utilization was increased and paralleled by an increase in lactate release. This stimulation of glycolysis by hypoxia and the corollary inhibition of anaerobic glycolysis by oxidative metabolism is termed the *Pasteur effect*.
- *1895*: Oscar Langendorff demonstrates that the mammalian heart receives oxygen and nutrients through coronary circulation.
- *Early 1900s*: Ernest Starling discovers that in normally oxygenated hearts, glucose contributes only a small amount to the fuel of the heart, in the absence of insulin.
- *1904*: Ludwig Winterstein discovers the oxygen dependency of the contracting mammalian heart.
- *1904*: Franz Knoop discovers  $\beta$ -oxidation of fatty acids, the metabolic oxidation at the  $\beta$ -carbon atom of a long-chain fatty acid by successive cycles of reactions, during each of which the fatty acid is shortened by a two-carbon-atom fragment removed as acetyl-coenzyme A.
- *1924*: Otto Warburg describes the nature and function of mitochondrial respiratory enzymes. He discovers that a fundamental difference between normal and cancerous cells is the ratio of glycolysis to respiration; this observation is known as the *Warburg effect*. The concept that cancer cells switch from oxidative metabolism to glycolysis has become widely accepted and is the basis of  $^{18}\text{F}$ -FDG positron emission tomography (PET) imaging today.
- *1930s*: C. Lovatt Evans et al. find that lactate can be readily taken up and oxidized as a fuel in the normally oxygenated heart.
- *1937*: Hans A. Krebs discovers the major metabolic cycle—known as the *Krebs cycle*, or the *citric acid cycle*—which represents the second of the three steps that convert fatty acids, glucose, and other fuels in the body into energy in the form of adenosine triphosphate (ATP).
- *1937*: Fritz A. Lipmann discovers the importance of ATP as the main energy carrier in cells; he later shared the 1953 Nobel Prize for Physiology or Medicine with Hans Krebs for his discovery of coenzyme A (CoA), a crucial link between glycolysis, the first stage in the process, and the Krebs cycle, and its importance for intermediary metabolism.
- *1950s*: Richard J. Bing, using coronary sinus cannulation and precise coronary artery flow measurements in the human heart, discovers the concept of the heart as a metabolic omnivore.
- *1960s*: Philip J. Randle discovers that fatty acids suppress glucose oxidation by inhibiting pyruvate dehydrogenase in the isolated perfused heart.
- *1960s*: Richard J. Bing introduces positron-emitting tracers for the measurement of blood flow.

## Metabolic Radiotracers

By labeling various compounds of physiologic interest, valuable insights into biochemical pathways and tissue metabolism can be obtained in functional and dysfunctional myocardium (Table 9.1). Currently, the only PET myocardial metabolic radiotracer approved by the US Food and Drug Administration (FDA) and reimbursable by the Centers for Medicare & Medicaid Services is  $^{18}\text{F}$ -fluoro,2-deoxy-D-glucose (FDG), which is the current gold standard for evaluating glucose metabolism, and myocardial viability. FDG is a glucose analogue that competes with glucose for phosphorylation by hexokinase. Once phosphorylated, it is trapped inside the cell and can be neither further metabolized nor exported back out of the cell. To assess fatty acid utilization, earlier studies used the labeled substrate  $^{11}\text{C}$ -palmitate, which is a PET-radiolabeled straight-chain fatty acid. After its uptake into the cell and activation by binding to coenzyme A,  $^{11}\text{C}$ -palmitate undergoes  $\beta$ -oxidation, ultimately leading to the release of  $^{11}\text{CO}_2$ . However, this technique requires a PET camera and an onsite cyclotron. As single-photon emission computed tomography (SPECT) cameras were already available to most nuclear cardiologists, the focus turned to the development of SPECT tracers for fatty acid oxidation. One of them is [ $^{123}\text{I}$ ]- $\beta$ -methyl-*p*-iodophenyl-pentadecanoic acid ( $^{123}\text{I}$ -BMIPP), a substrate analogue that is rapidly taken up into the cardiomyocytes and shows prolonged retention due to limited catabolism. Both  $^{123}\text{I}$ -BMIPP and  $^{11}\text{C}$ -palmitate interrogate myocardial fatty acid metabolism *in vivo*. The uptake and clearance of  $^{11}\text{C}$ -palmitate from the myocyte occurs quite rapidly via  $\beta$ -oxidation, whereas the methyl chain in  $^{123}\text{I}$ -BMIPP results in metabolic trapping of the radiotracer in the myocyte. A PET-radiolabeled short-chain acid that is ideal for the *in vivo* assessment of myocardial oxidative metabolism is  $^{11}\text{C}$ -acetate.

| Radiotracer                               | Assessment            |
|---|-----------------------|
| <i>SPECT radiotracers</i>                 |                       |
| $^{123}\text{I}$ -BMIPP                   | Fatty acid uptake     |
| $^{18}\text{F}$ -THA                      | Fatty acid uptake     |
| <i>PET radiotracers</i>                   |                       |
| $^{11}\text{C}$ -palmitate                | Fatty acid metabolism |
| $^{11}\text{C}$ -acetate                  | Oxidative metabolism  |
| $^{18}\text{F}$ -fluoro,2-deoxy-D-glucose | Glucose uptake        |
| $^{11}\text{C}$ -glucose                  | Glucose oxidation     |
| $^{11}\text{C}$ -glutamate                | Amino acid metabolism |
| $^{13}\text{N}$ -glutamate                | Amino acid metabolism |
| $^{11}\text{C}$ -methionine               | Amino acid metabolism |

$^{18}\text{F}$ -THA F-thiaheptadecanoic acid (FTHA)

**Table 9.1** Single-photon and positron-emitting metabolic radiotracers

Changes in fatty acid and glucose metabolism have been long-established parts of metabolic remodeling in various forms of heart disease, but much less is known about the alterations in amino acid metabolism and their impact on the onset and progression of cardiac disease.  $^{11}\text{C}$ -glutamate or  $^{13}\text{N}$ -glutamate are also useful for tracing the footprints of myocardial ischemia, and the uptake of  $^{11}\text{C}$ -methionine in infarcted areas during the acute phase after myocardial infarction is a useful tool in monitoring the remodeling of the heart after myocardial infarction.

Figures 9.2, 9.3, and 9.4 illustrate the metabolic pathways in the heart and the ways that radiotracers and tracer analogues can assess perfusion, substrate uptake, and other evidence of metabolic activity. The flux of energy is limited to a series of moiety-conserved cycles (Fig. 9.2).

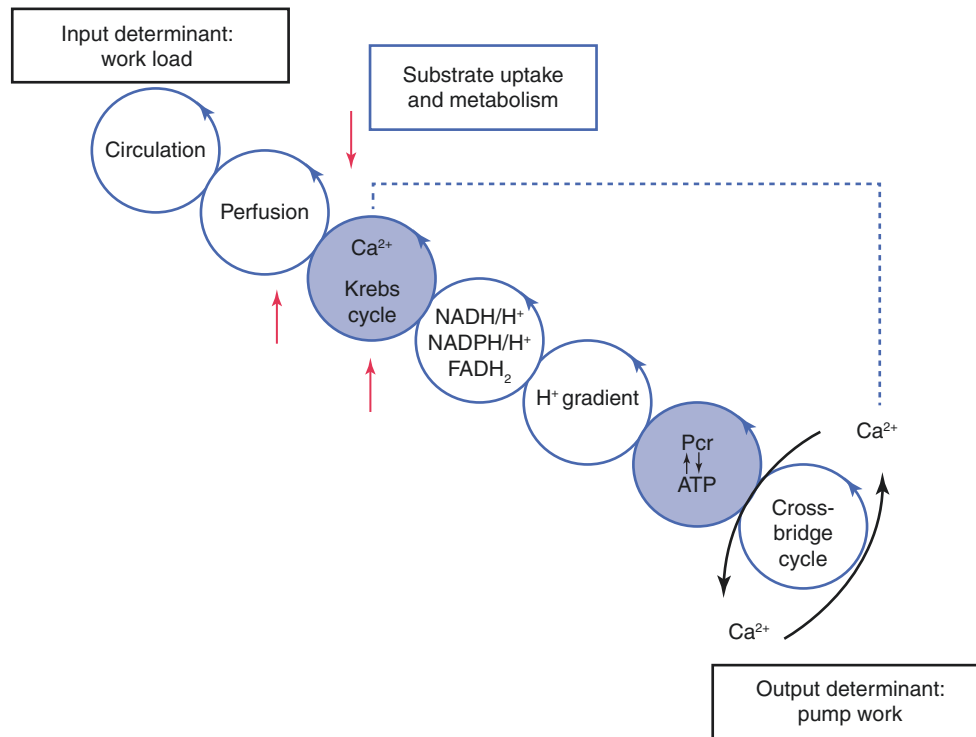


**Fig. 9.2** Energy is transferred along a series of moiety-conserved cycles, starting at coronary circulation and ending at the cross-bridge formation of contractile elements [7]. Nuclear metabolic imaging uses targeted radiotracers to assess flux through specific metabolic pathways (by quantifying either the flux of energy-providing substrates or the steady-state metabolites). Radiotracer retention and/or metabolism are assessed by noninvasive techniques such as single-photon emission computed tomography (SPECT) and positron emission tomography (PET). It is convenient to follow energy transfer in the heart muscle cells from the circulation (substrate and  $\text{O}_2$  delivery) to the cross bridges (energy utilization) through a series of moiety-conserved cycles. Specific radiotracers are available to assess perfusion and substrate

uptake and delivery, as well as Krebs cycle turnover (oxygen consumption). Radiolabeled tracers in combination with SPECT or PET (*red arrows*) and nuclear magnetic resonance spectroscopy with either stable isotopes (e.g.,  $^{13}\text{C}$ ) or  $^{31}\text{P}$  (*blue cycles*) can assess various cycles noninvasively in vivo. Calcium ( $\text{Ca}^{2+}$ ) is not an imaging agent, but the ion has been included because it is the signal that links contraction and mitochondrial respiration. Calcium release from the sarcoplasmic reticulum triggers calcium uptake into the mitochondria and activation of dehydrogenases in the Krebs cycle [7].  $\text{FADH}_2$  reduced flavin adenine dinucleotide,  $\text{NADPH}/\text{H}^+$  reduced nicotinamide adenine dinucleotide (phosphate), PCr phosphocreatine. From Osterholt et al. with permission [7]



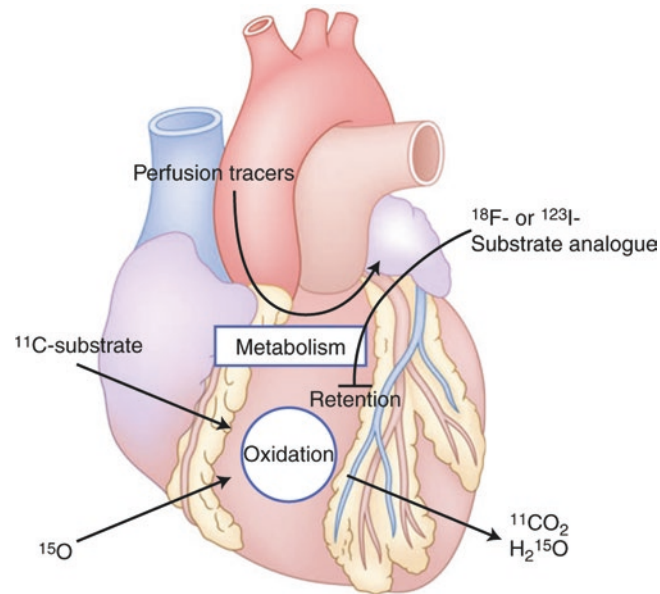


**Fig. 9.3** Overview of the fate of labeled substrates and substrate analogues. Two classes of radiotracers are currently used to trace metabolic activity: labeled substrates or substrate analogues. Labeled substrates are taken up by heart muscle and either rapidly cleared or retained, whereas substrate analogues are taken up and retained only. Radiolabeled  $^{11}\text{C}$ -substrate is taken up into the cell and undergoes

complete oxidation, eventually leading to the release of  $^{11}\text{CO}_2$ . After their uptake into the cell, substrate analogues labeled with  $^{18}\text{F}$  or  $^{123}\text{I}$  are partially metabolized and then retained. The majority of perfusion tracers require preserved cellular metabolism to be taken up by the cell. Substrate oxidation rates can also be monitored using  $^{15}\text{O}$  and measuring the release of  $\text{H}_2^{15}\text{O}$ . Adapted from Osterholt et al. [7] with permission

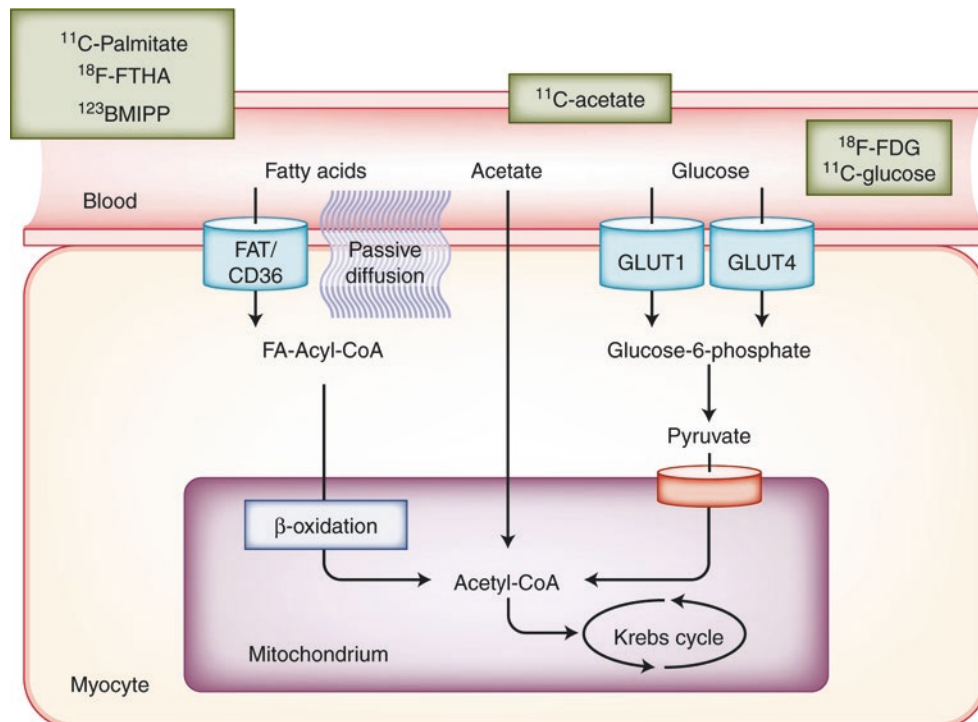


**Fig. 9.4** Imaging the main pathways of cardiac metabolism. Fatty acid, glucose, and oxidative metabolism assessment with various SPECT and PET radiotracers is shown. Free fatty acids account for most ATP production when the heart is in a normal, fasting state. Following uptake of the radiotracers by active transport or diffusion, fatty acids are converted by  $\beta$ -oxidation into acetyl-coenzyme A (CoA). Under anaerobic or nonfasting conditions, energy production shifts to glucose metabolism. The conver-

sion of glucose via glucose-6-phosphate and pyruvate provides the source of acetyl-CoA. Oxidative metabolism also provides an important contribution to cardiac metabolism. In mitochondria, ATP production occurs via the tricarboxylic acid (TCA) cycle. BMIPP  $\beta$ -methyl p-[ $^{123}\text{I}$ ]-iodophenyl-pentadecanoic acid, FA fatty acid, FAT/CD36 fatty acid translocase, FDG fluorodeoxyglucose, FTHA  $^{18}\text{F}$ -thiaheptadecanoic acid, GLUT1 and GLUT4 glucose transporters 1 and 4, THA thiaheptadecanoic acid

## Metabolic Signals in Normal and Diseased Heart: Opportunities for Molecular Imaging

A refined understanding of metabolic regulation may result in the early diagnosis and treatment of subclinical myocardial ischemia and heart failure, as metabolic changes and changes in gene expression are likely to precede contractile dysfunction and other functional remodeling of the stressed heart (Figs. 9.5, 9.6, 9.7, 9.8, 9.9, 9.10, 9.11, and 9.12).

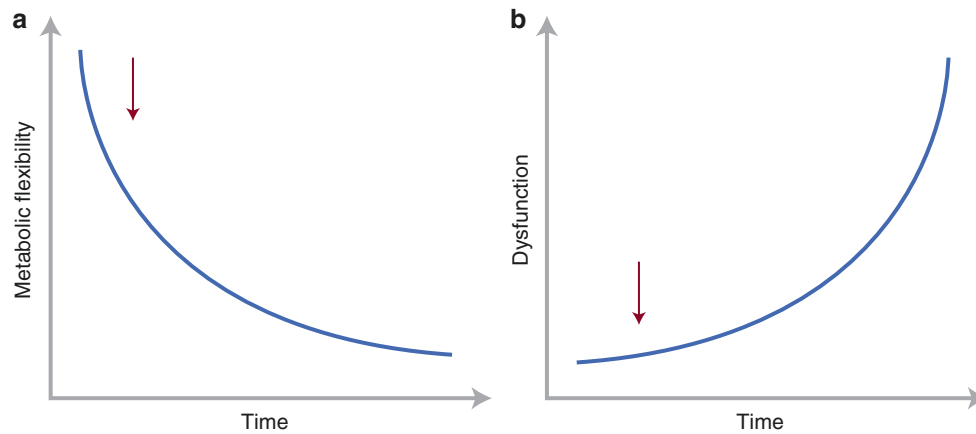


**Fig. 9.5** Metabolic regulation. These hyperbolic curves illustrate a hypothetical time course of the rapid loss of metabolic flexibility antedating contractile dysfunction in the path of metabolic and functional remodeling of the stressed heart. The loss of metabolic flexibility (**a**, *arrow*) and changes in gene expression likely precede the onset of

severe contractile dysfunction (**b**, *arrow*) [3]. The concept depicted in this figure is supported by the observation that transcriptional changes of enzymes and proteins of energy substrate metabolism antedate any contractile dysfunction in hearts from diabetic animals [8]

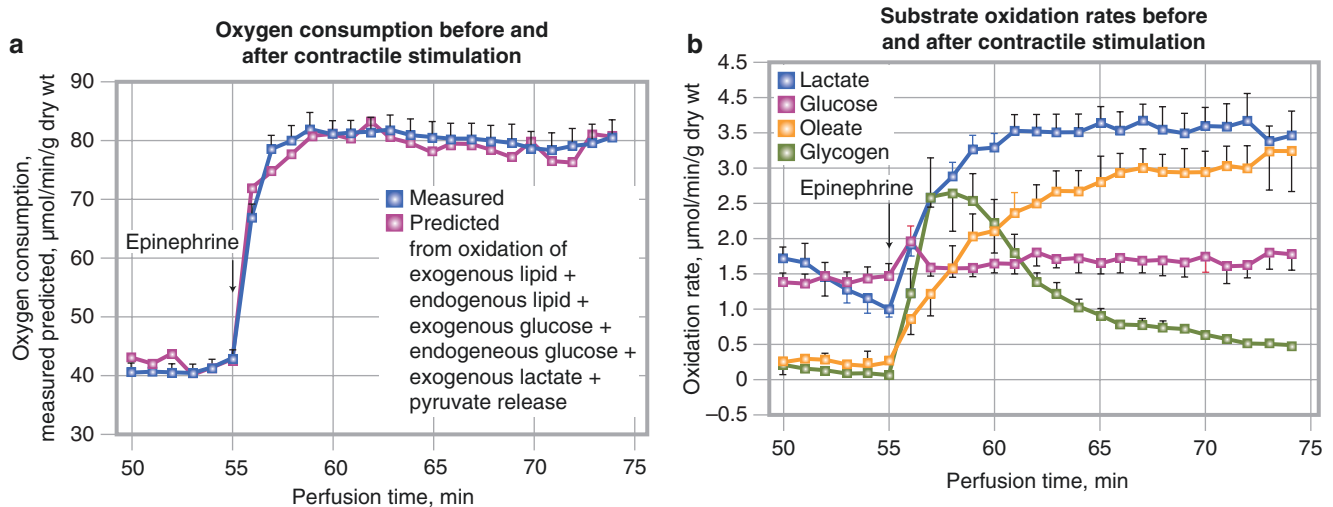


**Fig. 9.6** (a) Measured and predicted values for oxygen consumption. Predicted rates are based on the sum of the measured rates of oxygen of every major substrate (glucose, glycogen, lactate, oleate, triglycerides, and release of pyruvate). The close agreement between measured and predicted  $\text{MVO}_2$  validates the assumption of uniform isotopic dilution, and that every major oxidizable substrate was quantitatively accounted for in the heart. (b) Rates of substrate oxidation before and after inotropic stimulation. Fuel selection during acute transition from low to high workload ( $1 \mu\text{M}$  epinephrine and afterload increase by 40%) of isolated working rat heart is shown. When the workload is acutely increased, glycogen and, to a lesser extent, lactate become the most important energy substrates for the aerobic heart (a). With more prolonged adrenergic stimulation, nonesterified fatty acids and lactate are the major respiratory substrates for the heart, which is in keeping with the *in vivo* observations in the exercising state. When all relevant exogenous and endogenous substrates are examined, the increase in carbohydrate oxidation upon adre-

nergic stimulation is selective. Although exogenous fatty acid oxidation is not significantly changed, total  $\beta$ -oxidation increases by 40%, and the increase is associated with a decrease in the level of malonyl-coenzyme A (CoA). Carbohydrate oxidation is increased selectively because total  $\beta$ -oxidation, regulated mostly by malonyl-CoA levels in the cytosol, is independent of the activity of pyruvate dehydrogenase complex in the mitochondria. Using values of the distribution between oxidation and the release of lactate or pyruvate during adrenergic stimulation, the calculated effective value of the ATP synthesized/ $\text{O}_2$  consumed ratio (not to be confused with the ATP/ $\text{O}_2$  ratio calculated for complete oxidation) is 5.4 for glucose and 5.7 for glycogen, which is higher than those ratios calculated for oleate (5.0) and lactate (4.8). The higher ATP yield with glycogen during periods of high energy demand provides a potential explanation for why the heart adopts the strategy of preferential increase in carbohydrate oxidation to deal with increased energy demand. From Goodwin et al. with permission [9]



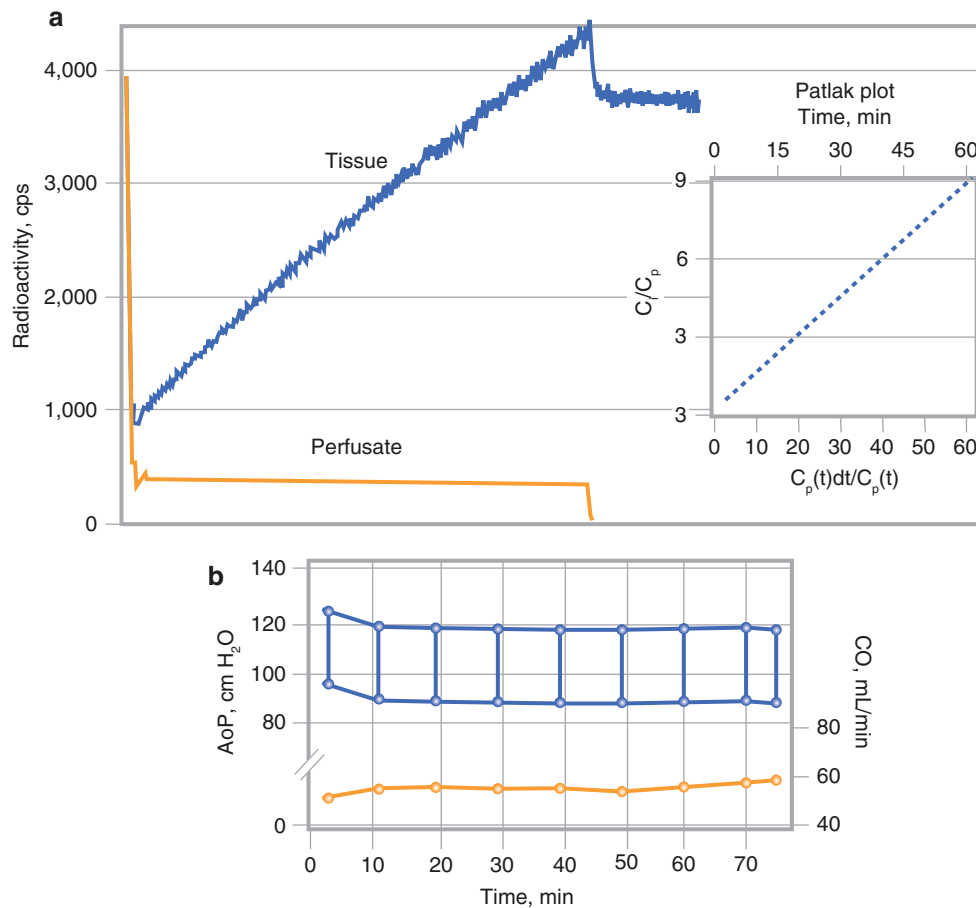


**Fig. 9.7** Direct evidence that fluorodeoxyglucose (FDG) uptake traces glucose metabolism and that FDG is retained by the tissue in proportion to the rate of glucose utilization. The underlying premise of FDG PET imaging is that FDG behaves similarly to the traced substrate (glucose) with respect to facilitated transport across the sarcolemma and subsequent intracellular phosphorylation by hexokinase. The time-activity curves shown were obtained in an isolated working rat heart (after-load = 100 cm H<sub>2</sub>O; preload = 15 cm H<sub>2</sub>O) with Krebs–Henseleit saline containing glucose (10 mM) and FDG (350  $\mu$ Ci/200 mL perfusate) for the first 60 minutes. After an initial phase of tracer equilibrium (a), the myocardial uptake of FDG is linear (*top curve*), whereas tracer activity in the perfusate remains constant (*bottom curve*). Graphical analysis of the myocardial and perfusate FDG concentrations acquired between 5 and 60 minutes by Patlak analysis (*inset in a*) shows a linear plot from 20 to 60 minutes. Aortic pressures (AoP) and cardiac output (CO) are

stable throughout the experiment (b). At 60 minutes, when the perfusion medium was changed to a buffer containing no tracer, radioactivity in the tissue fell abruptly and then remained stable for the duration of the washout period. The phenomena described above indicate clearance of the radiotracer from the heart chambers and the vascular and extracellular spaces, as well as metabolic trapping of FDG. Not shown in the figure is that tissue accumulation of FDG decreased with a reduction in work load and with the addition of competing substrates, and that insulin caused a significant increase in FDG accumulation in hearts from fasted (but not from fed) animals. These data confirm the utility of FDG to assess myocardial glucose metabolism in the clinical setting by showing that tissue uptake and retention of the tracer in the isolated working rat heart responds to physiologic interventions in the same way as glucose. Adapted from Nguyen et al. with permission [10]

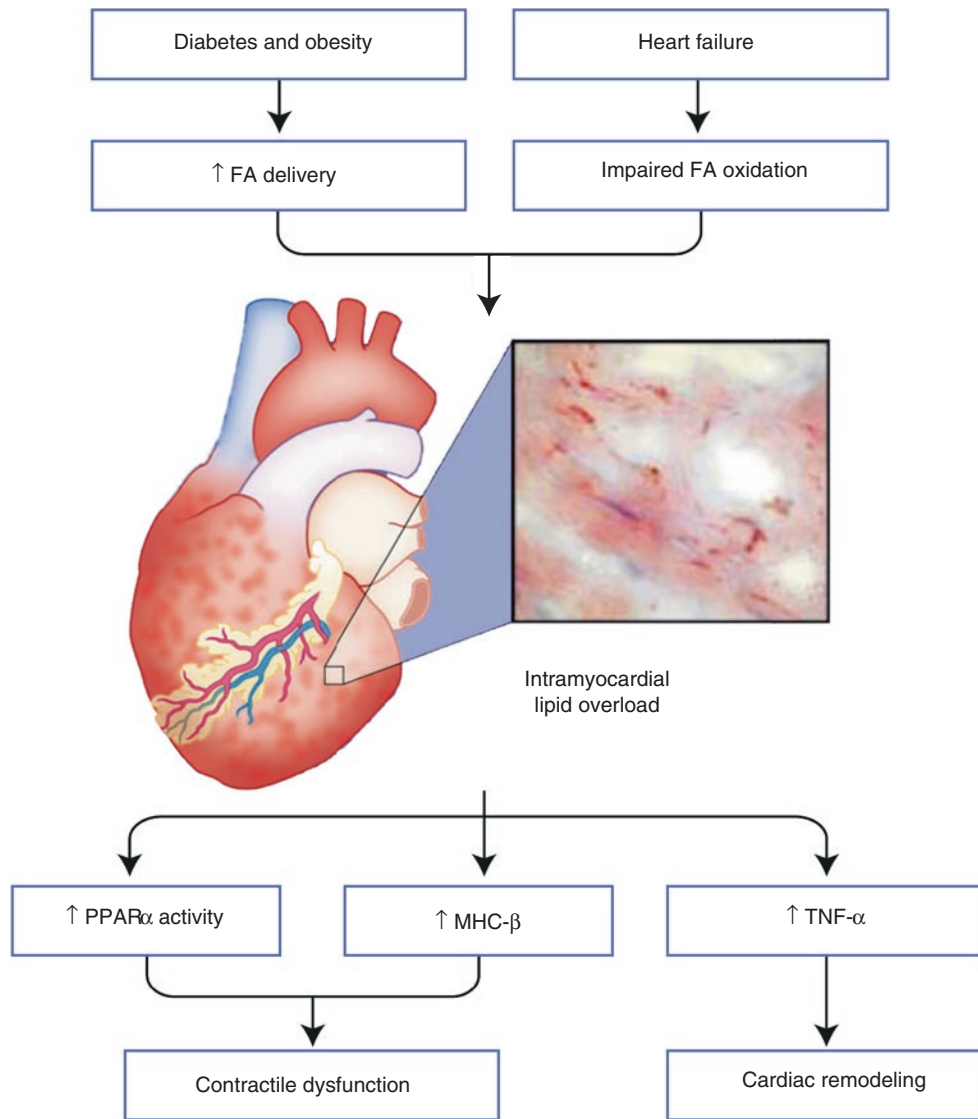


**Fig. 9.8** Myocardial lipid accumulation in heart failure and diabetes. Left ventricular dysfunction in patients with diabetes and/or obesity or heart failure is associated with altered metabolism independent of the presence of underlying coronary artery disease. Although patients with a similar glycemic control (HbA1c) may have dramatically different rates of left ventricular dysfunction, both increased fatty acid (FA) delivery (e.g., diabetes, obesity) or impaired fatty acid (FA) oxidation

(e.g., heart failure) result in severe intramyocardial triglyceride accumulation. Triglycerides are like a “canary in the coal mine” reflecting a host of other lipotoxic intermediates, including oxygen-derived free radicals, diacylglycerol, and ceramide. An oil-red-O stain of triglycerides is shown in failing heart muscle [11]. MHC- $\beta$  myosin heavy chain- $\beta$ , PPAR $\alpha$  peroxisome proliferation-activated receptor  $\alpha$ , TNF- $\beta$  tumor necrosis factor- $\beta$

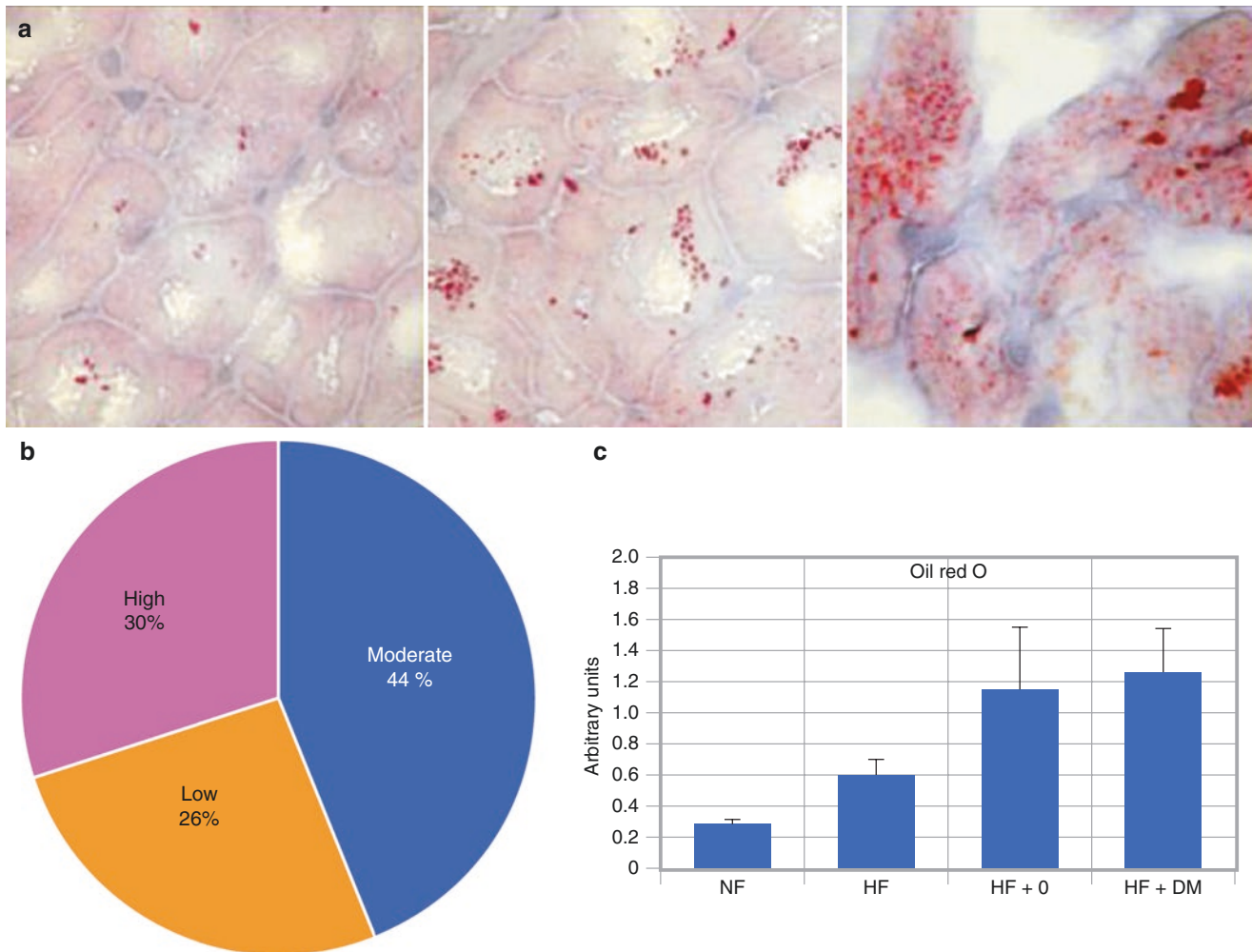


**Fig. 9.9** Intramyocardial triglyceride overload. Intramyocardial triglyceride overload and changes in gene expression are associated with contractile left ventricular dysfunction in patients with nonischemic heart failure. (a) Low, intermediate, and high intramyocardial lipid accumulation can be appreciated histologically in heart tissue samples from these patients. (b) In a study of 27 nonischemic failing hearts, high amounts of intramyocardial lipid overload were present in 30% of hearts. (c) The highest levels of lipid staining were observed in the hearts of patients with heart failure (HF) with coexisting diabetes mellitus (DM) or obesity (O, body mass index >30). Intramyocardial lipid deposition was associated with an upregulation of peroxisome

proliferation-activated receptor (PPAR)  $\alpha$ -regulated genes, myosin heavy chain- $\beta$ , and tumor necrosis factor- $\alpha$ . Intramyocardial lipid overload is a relatively common finding in nonischemic heart failure and is associated with a distinct gene expression profile that is similar to an animal model of lipotoxicity and cardiac dysfunction. Metabolic imaging may play an important role for detecting subclinical disease early in the process of left ventricular dysfunction and/or remodeling. Early identification may be more amenable to medical therapies such as PPAR agents, insulin, and fish oil analogues, and in prevention [11]. NF nonfailing. Adapted from Sharma et al. with permission [11]

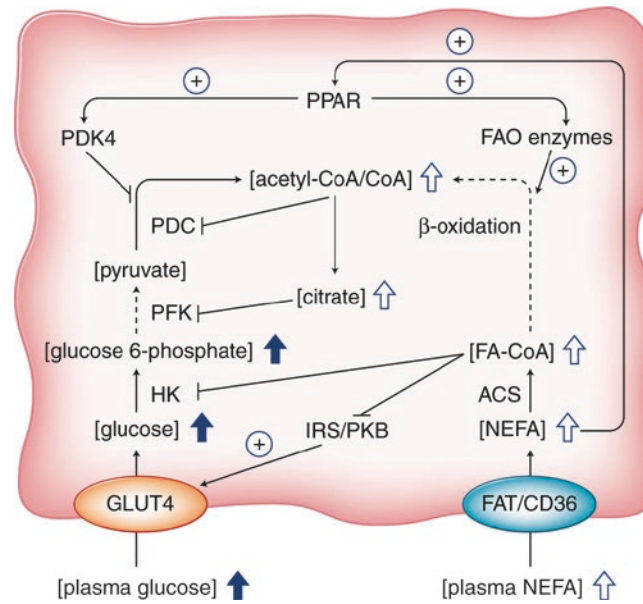


**Fig. 9.10** Proposed mechanisms for fatty acid inhibition of glucose oxidation. During diabetes, levels of both plasma glucose and plasma nonesterified fatty acid (NEFA) are elevated. The latter results in increased intracellular levels of fatty acids (FAs) and their fatty acyl-coenzyme A (FA-CoA) derivatives. FA-CoAs inhibit insulin-mediated glucose transport by inhibiting insulin receptor substrates (IRSs) and protein kinase B (PKB). FA-CoAs also can directly inhibit hexokinase (HK). Increased  $\beta$ -oxidation (due to increased substrate availability and increased gene expression of FA oxidation [FAO] enzymes via peroxisome proliferation-activated receptor [PPAR] activation) results in an

increase in the mitochondrial acetyl-CoA/CoA ratio. The combined effects of increased PDK4 expression (induced through FA activation of PPAR) and an increased acetyl-CoA/CoA ratio severely inhibit the pyruvate dehydrogenase complex (PDC). In addition, the increased acetyl-CoA/CoA ratio promotes citrate efflux from the mitochondrion into the cytosol, where it is able to inhibit phosphofruktokinase (PFK). Despite decreased insulin-mediated glucose transport, glucose uptake by the diabetic heart is comparable to uptake by the normal heart because of the hyperglycemia. Glycolytic intermediates therefore accumulate in the cardiomyocyte [12]

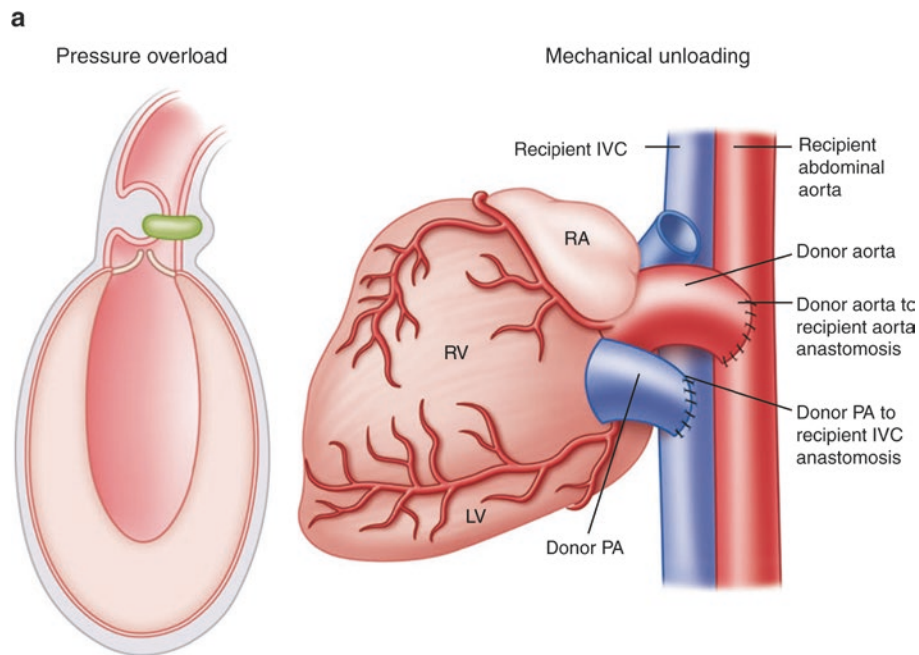


**Fig. 9.11** Metabolic processes are transcriptionally regulated in response to chronic changes in the workload of the heart. (a) The change in cardiac mass by both pressure overload and ventricular unloading is a mechanism of adaptation accompanied by the reexpression of fetal genes. However, cardiac hypertrophy, if not treated, evolves to an uncompensated state of heart failure, whereas the process of atrophy induced by ventricular unloading rapidly stabilizes and shows no further progression thereafter. Therefore, unloading the failing heart reduces cardiac mass by a self-limited process and limits energy expenditure by preserving the expression of fetal isoforms of proteins that are regulating myocardial energetics. These mechanisms may explain the clinical improvement of patients with heart failure after treatment with a left ventricular assist device (LVAD), but the true mechanisms remain unknown. The process of unloading the heart with an LVAD is now used in clinical practice for patients with advanced heart failure awaiting heart transplantation; mechanical unloading may improve cardiac function to an extent that makes transplantation no longer necessary. Such improvement results from a better contractile performance of the myocytes after LVAD intervention, which indicates that mechanical

unloading *in vivo* affects the expression of genes coding for contractile proteins and/or metabolic enzymes. These clinical results prompted investigators to assess the molecular response of the heart to unloading [13]. (b) The *top two panels* show the changes in left ventricular mass (lung volume/body weight [LV/BW] ratio) in response to pressure overload and unloading. The *lower panels* show the expression of  $\alpha$  myosin heavy chain ( $\alpha$ MHC),  $\beta$  MHC, SERCA 2a, and SK  $\alpha$ -actin in (1) hypertrophied hearts compared with hearts from sham-operated rats and (2) unloaded hearts compared with control hearts up to 28 days after transplantation. Data are reported as the number of mRNA transcripts per number of 36B4 molecules (constitutive housekeeping gene product). Both conditions induced a reexpression of growth factors and proto-oncogenes, as well as a downregulation of the “adult” isoforms but not of the “fetal” isoforms, of proteins regulating myocardial energetics. Therefore, opposite changes in the cardiac workload *in vivo* induce similar patterns of gene response. Ctrl—control; SERCA 2a—sarco-plasmic/endoplasmic reticulum  $\text{Ca}^{2+}$ ATPase 2a. (From Depre et al. [13]; with permission from Springer Nature)

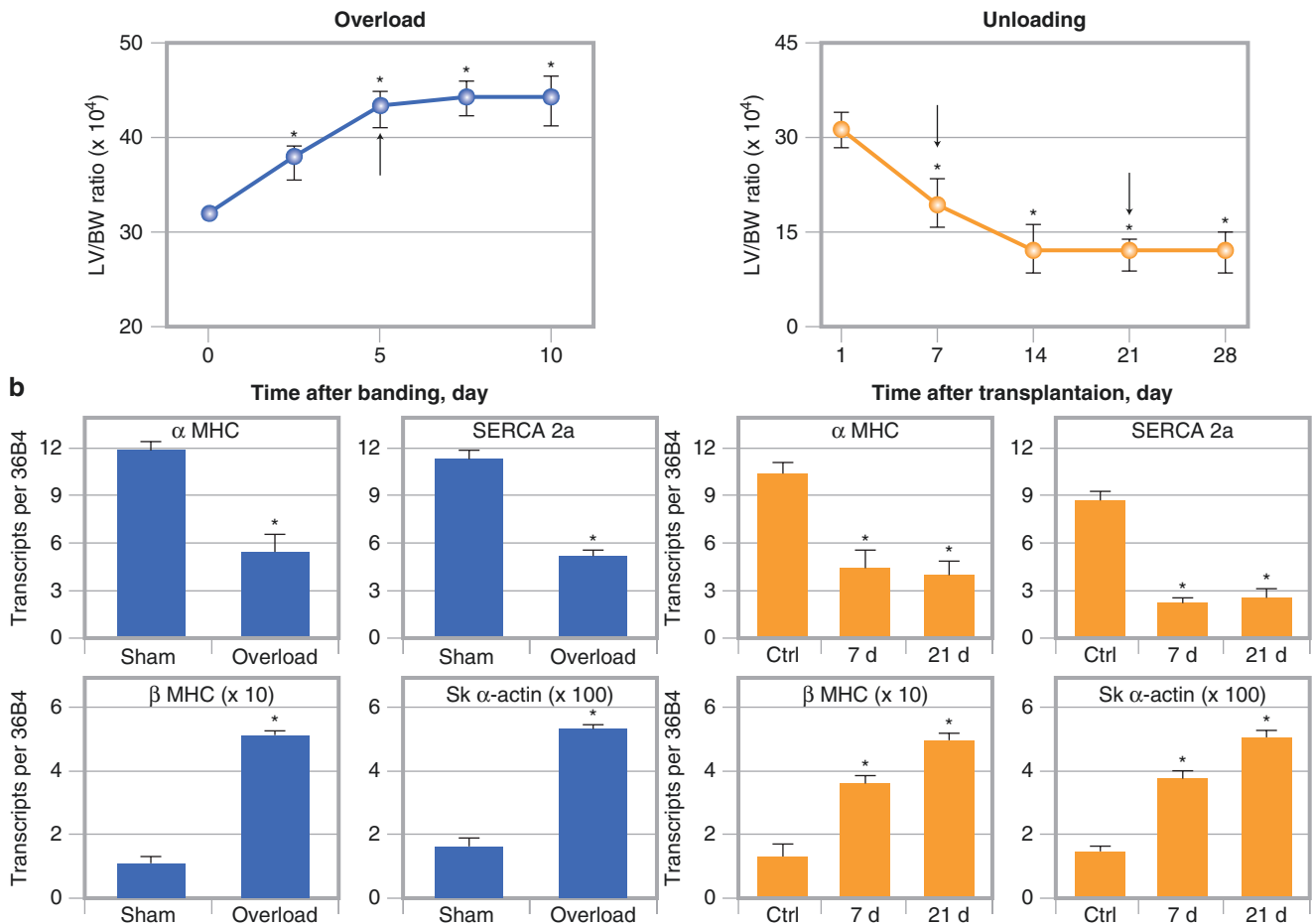


**Fig. 9.11** (continued)

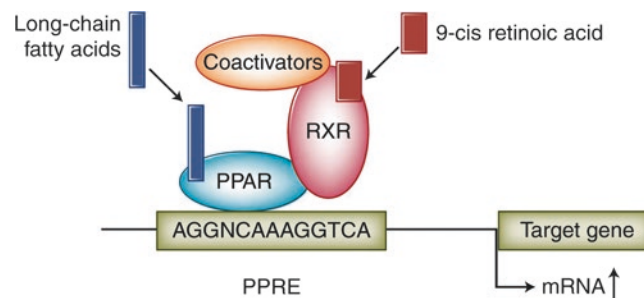


**Fig. 9.12** Peroxisome proliferation-activated receptor (PPAR)- $\alpha$  activation of target metabolic genes as an example for the ligand activation of a nuclear receptor by long-chain fatty acids. PPAR $\alpha$ , a transcription factor that modulates fatty acid metabolism, regulates substrate preference in the heart. In acute ischemia, there is a switch in substrate preference from fatty acids to glucose, but in response to repetitive ischemia, there is a reversible downregulation of the genes that modulate fatty acid metabolism and myosin heavy chain isoforms in the heart. When fatty acid metabolism is pharmacologically reactivated in hearts exposed to repetitive ischemia, there is worsening of contractile function, microinfar-

ctions, and triglyceride accumulation within cardiomyocytes. These findings suggest that downregulation of fatty acid metabolic gene expression in the hibernating myocardium is an adaptive mechanism. Furthermore, modulating the myocardial metabolism may provide a pharmacologic target for cardiac protection in repetitive ischemia. Further phenotypic characterization of genetic variables such as PPAR may play an important role in the future for drug development and individualized medicine [14]. PPRE peroxisome proliferator response element, RXR retinoid X receptor. Adapted from Sharma et al. with permission [11]



## Clinical Application of Myocardial Metabolism: PET and SPECT Techniques

### PET Techniques: $^{11}\text{C}$ -Palmitate

The principle of using a metabolic tracer for myocardial imaging is based on the concept that viable myocytes in hypoperfused and dysfunctional regions are metabolically active, whereas scarred or fibrotic tissue is metabolically inactive. Under fasting and aerobic conditions, long-chain fatty acids are the preferred fuel in the heart; they supply 65–70% of the energy for the working heart, and approximately 15–20% of the total energy supply comes from glucose. Thus, early studies have focused on using PET to characterize the myocardial kinetics of the long-chain fatty acid tracer  $^{11}\text{C}$ -palmitate. Uptake of  $^{11}\text{C}$ -palmitate by the heart is dependent on regional perfusion, diffusion across the sarcolemmal membrane, transporter protein, and acceptance in the cytosol by binding to coenzyme A (CoA). In normally perfused myocardium, the extraction fraction of  $^{11}\text{C}$ -palmitate is 40%. Transported across the sarcolemma by a transporter protein (CD36) of long-chain fatty acid, the myocyte fatty acids are bound to a binding protein. Metabolic activation of  $^{11}\text{C}$ -palmitate occurs through attachment to CoA. Depending on demand, about 80% of the extracted  $^{11}\text{C}$ -palmitate is activated for transport from the lipid pool into the mitochondria (via the carnitine shuttle) for breakdown by  $\beta$ -oxidation, which results in the generation of carbon dioxide that appears in the venous effluent of the coronary circulation in less than a minute after  $^{11}\text{C}$ -acyl-CoA transfers into the mitochondria (Fig. 9.13). Following is a summary of the PET technique:

- Image acquisition starts at 15–20 mCi bolus injection of the tracer and continues 40–60 minutes.
- Initial uptake and distribution in the myocardium is determined primarily by regional blood flow.
- In the cytosol,  $^{11}\text{C}$ -palmitate is esterified to  $^{11}\text{C}$ -acyl-CoA, which is mediated by thiokinase, an energy-dependent reaction, resulting in trapping of the tracer in the myocardium.
- Thereafter,  $^{11}\text{C}$ -acyl-CoA either enters the endogenous lipid pool as  $^{11}\text{C}$  glycerides and  $^{11}\text{C}$  phospholipids or moves via the carnitine shuttle to the mitochondria, where rapid degradation by  $\beta$ -oxidation results in the generation of carbon dioxide.

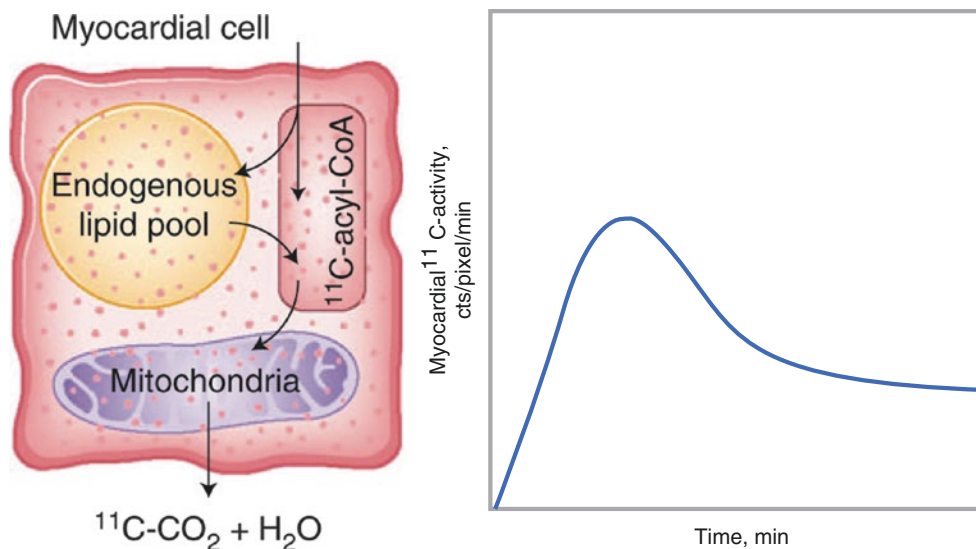


**Fig. 9.13** PET of  $^{11}\text{C}$ -palmitate. External measurement by dynamic PET imaging allows the observation of tracer inflow, peak accumulation, and release of the tracer within a particular region of interest in the

myocardium. Fatty acid imaging with radioiodine-labeled fatty acid analogues such as  $^{125}\text{I}$ -BMIPP using SPECT is also possible [15]

### SPECT Technique: $^{123}\text{I}$ -BMIPP

Alterations in myocardial fatty acid metabolism were first evaluated noninvasively in humans using  $^{14}\text{C}$ -palmitate, which requires an onsite cyclotron and a PET camera. Because most nuclear cardiology laboratories are equipped with SPECT cameras, investigators subsequently focused their attention on developing gamma-emitting fatty acid tracers. In contrast to palmitate,  $\beta$ -methyl- $p$ - $^{123}\text{I}$ -iodophenyl-pentadecanoic acid ( $^{123}\text{I}$ -BMIPP) is an iodine-labeled, methyl branched-chain fatty acid that is predominantly trapped in myocardial cells with limited catabolism. Uptake of BMIPP from the plasma into myocytes occurs via the CD36 transporter protein present on the sarcolemmal membrane (Fig. 9.14). Once in the cell, BMIPP will either back-diffuse to the plasma, accumulate in the lipid pool, or undergo limited  $\alpha$ - and  $\beta$ -oxidation. Enzymatic conversion of BMIPP to BMIPP-CoA or triacylglycerol in the myocyte is ATP-dependent and is an irreversible step. Such conversion prevents the back-diffusion of BMIPP to the plasma and facilitates its cellular retention. The prolonged retention of BMIPP in the myocardium, combined with rapid clearance from the blood and diminished uptake in the liver and lung, results in excellent visualization and imaging of the myocardium by SPECT techniques. Thus, BMIPP provides a means of measuring myocardial fatty acid utilization *in vivo*. In the setting of myocardial ischemia, a reduction in ATP production secondary to diminished fatty acid metabolism is mirrored by decreased myocardial BMIPP uptake. BMIPP is approved for clinical use in Japan, but it has not yet received approval by the US FDA.

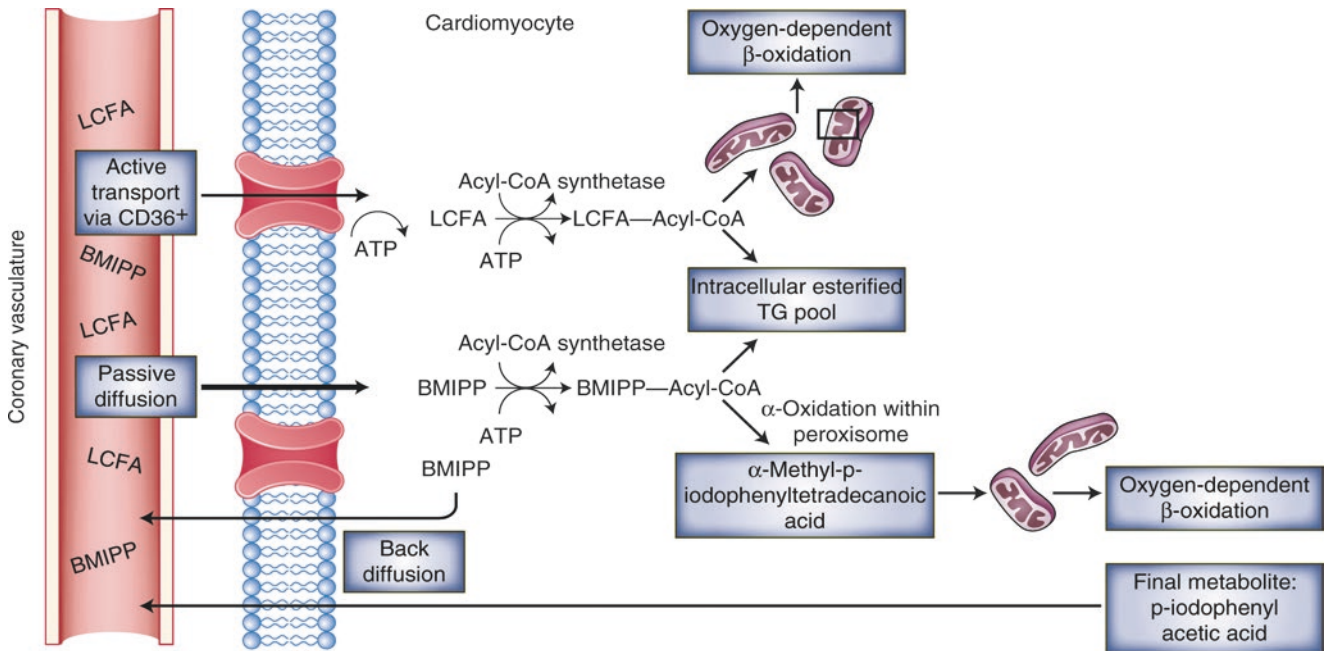


**Fig. 9.14** Major metabolic pathways and regulatory steps of BMIPP in the myocyte. Under normoxic conditions, the myocardium preferentially oxidizes long-chain fatty acids (LCFAs) to generate ATP. Fatty acids enter the endothelial cell via diffusion or active transport through integral CD36<sup>+</sup> membrane-bound proteins. The ATP-dependent activation of fatty acids by acyl-CoA synthetase involves its transformation to acyl-CoA moieties that can then undergo  $\beta$ -oxidation in the mitochondria. The majority of LCFA-acyl-CoA derivatives are metabolized via  $\beta$ -oxidation, whereas the remainder of the acyl-CoA and acyl moieties are incorporated into the intracellular esterified triglyceride (TG) pool. BMIPP, however, is not initially metabolized by  $\beta$ -oxidation because

the methyl substitution precludes the formation of the keto-acyl-CoA intermediate. BMIPP must first undergo an obligatory initial  $\alpha$ -oxidation conversion step in the cytosol or primarily the peroxisome, to  $\alpha$ -methyl- $p$ -iodophenyl-tetradecanoic acid (AMIPT). AMIPT is metabolized by rounds of  $\beta$ -oxidation in the mitochondria to the end product, 2-( $p$ -[ $^{123}\text{I}$ ] I-iodophenyl) acetic acid, which does not accumulate intracellularly. BMIPP appears to be primarily activated (esterified-CoA) in the cytosol and incorporated into triglyceride storage products into the endogenous lipid pool (70%). BMIPP, if not activated, can undergo early washout back into the bloodstream [16]

## PET Technique: $^{11}\text{C}$ -Acetate

$^{11}\text{C}$ -acetate is a short-chain fatty acid that is avidly extracted by the myocardium, with a first-pass extraction of 63% at blood flows of 1 mL/g/min. It is metabolized predominantly by mitochondrial oxidation. Once in the cytosol, the tracer is converted to acetyl-CoA by acetyl-CoA synthetase and is oxidized by the Krebs cycle in the mitochondria to  $^{11}\text{C}$ -carbon dioxide and water. Thus, the washout rate of  $^{11}\text{C}$ -acetate from myocardium is directly related to the oxidative metabolism. Given the close link between the Krebs cycle and oxidative phosphorylation, the myocardial turnover and clearance of  $^{11}\text{C}$ -acetate in the form of  $^{11}\text{C}$ -carbon dioxide may reflect overall oxidative metabolism and provide insight into the mitochondrial function of viable myocardium (Fig. 9.15). Alternative metabolic pathways of  $^{11}\text{C}$ -acetate include incorporation into amino acids, ketone bodies, and fatty acids by de novo synthesis or chain elongation, but these latter pathways are thought to be modest and unlikely to compromise estimation of regional myocardial oxygen consumption per minute.

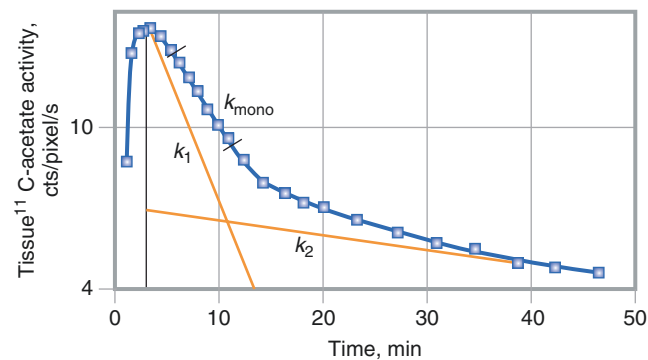


**Fig. 9.15** Myocardial  $^{11}\text{C}$ -acetate tissue time-activity curve demonstrating biexponential clearance of the tracer from myocardium. Monoexponential fitting of the early portion of the clearance phase yields the slope  $k_{\text{mono}}$ , while biexponential least-square fitting of the clearance phase yields  $k_1$  and  $k_2$  slopes. The rapid phase of clearance ( $k_1$ ) represents oxidation of extracted  $^{11}\text{C}$ -acetate by the mitochondria to  $^{11}\text{C}$ -carbon dioxide, and the slower phase of clearance ( $k_2$ ) represents the incorporation of  $^{11}\text{C}$ -acetate into amino acids and other alternative metabolic pathways. In patients with recent myocardial infarction and chronic stable angina, the preservation of myocardial oxidative metabo-

lism is shown to predict functional recovery after revascularization [17, 18]. When clearance rates of  $^{11}\text{C}$ -acetate are within two standard deviations of the normal mean, the positive predictive accuracy for recovery of function after revascularization is 84% in patients with recent myocardial infarction and 79% in patients with chronic stable angina. Conversely, when clearance rates of  $^{11}\text{C}$ -acetate are more than two standard deviations below the normal mean, the negative predictive values are 70% in patients with recent myocardial infarction and 83% in patients with chronic stable angina [19]

## PET and SPECT Techniques: $^{18}\text{F}$ -FDG

$^{18}\text{F}$ -fluorodeoxyglucose (FDG) is a glucose analogue used to image myocardial glucose utilization with PET. Following an intravenous injection of 5–10 mCi FDG, FDG rapidly exchanges across the capillary and cellular membranes and is phosphorylated by hexokinase to FDG-6-phosphate. Once phosphorylated, FDG is not metabolized further in the glycolytic pathway, fructose-pentose shunt, or glycogen synthesis. Because the dephosphorylation rate of FDG is slow, essentially it becomes trapped in the myocardium, allowing adequate time to image regional glucose uptake by PET or SPECT. In the fasting and aerobic conditions, fatty acids are the preferred source of myocardial energy production, with glucose accounting for some 15–20% of the total energy supply. In the fed state, however, plasma insulin levels increase, glucose metabolism is stimulated, and tissue lipolysis is inhibited, resulting in reduced fatty acid delivery to the myocardium. The combined effects of insulin on these processes and the increased arterial glucose concentration associated with the fed state result in preferred glucose utilization by the myocardium. Myocardial FDG uptake is influenced by metabolic and hormonal milieu, workload, and blood flow.

The diagnostic quality of FDG imaging is critically dependent on a number of factors, such as hormonal milieu, substrate availability, and regional blood flow [20]. This becomes particularly evident when studying patients with clinical or subclinical diabetes. Most clinical studies are performed after 50–75 g glucose loading with oral dextrose approximately 1–2 hours before the FDG injection. Although 90% of FDG images are of adequate to excellent diagnostic quality in nondiabetic patients, the quality of FDG images after glucose loading is less certain in patients with clinical or subclinical diabetes mellitus. Because the increase in plasma insulin levels after glucose loading may be attenuated in patients with diabetes mellitus, tissue lipolysis is not inhibited and free fatty acid levels in the plasma remain high. The quality of FDG images in diabetics may be optimized by the use of standardization schemes:

- Intravenous bolus of regular insulin
  - Most common and clinically feasible approach
  - Regular insulin is administered according to plasma glucose level and a predetermined sliding scale.
  - Plasma glucose level is assessed every 15 minutes, with the administration of additional boluses of insulin, if necessary.
  - FDG dose is injected once the plasma glucose level is below 140 mg/dL.
- Hyperinsulinemic–euglycemic clamping
  - Insulin and glucose are infused simultaneously to achieve a stable plasma insulin level of 100–120 IU/L and a normal plasma glucose level.
  - The rate of glucose infusion (20% dextrose solution with potassium chloride) is adjusted intermittently based on measured glucose levels.
  - Although it provides excellent image quality, this technique is rather tedious and impractical for routine clinical studies.
- Use of nicotinic acid derivative
  - Approximately 2 hours before the FDG dose injection, a single dose of nicotinic acid derivative is given orally, followed by glucose loading.
  - FDG image quality is comparable to that obtained after the clamping technique in the same patient population.

## Metabolic Pathways and Patterns

The major metabolic pathways, as outlined in Fig. 9.16, offer opportunities to evaluate myocardial perfusion patterns with the use of PET and SPECT imaging and other techniques to find subclinical defects and determine whether myocardium remains viable after ischemia or infarction (Figs. 9.17, 9.18, 9.19, 9.20, 9.21, 9.22, 9.23, 9.24, 9.25, 9.26, and 9.27). An advantage of PET is that it can be safely performed in patients with an implanted cardiac defibrillator or renal insufficiency.

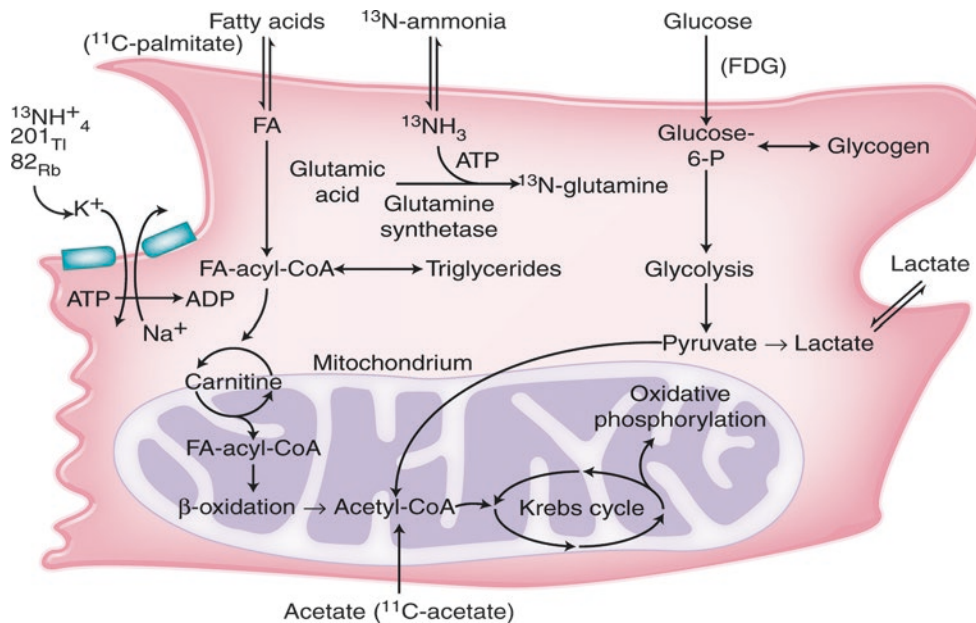


**Fig. 9.16** Major metabolic pathways and regulatory steps of a myocyte. Breakdown of fatty acids in the mitochondria via  $\beta$ -oxidation is exquisitely sensitive to oxygen deprivation. Therefore, in the setting of reduced oxygen supply, the myocytes compensate for the loss of oxidative potential by shifting toward greater utilization of glucose to generate high-energy phosphates. Glycolysis occurs in the cytoplasm under anaerobic conditions and leads to the formation of pyruvate. For every mol of glucose metabolized through glycolysis, 2 mol of ATP are generated (anaerobic condition), and 36 mol of ATP are generated from pyruvate entering the Krebs cycle rate in the mitochondria. Protons are generated for oxidative phosphorylation. Because glycolysis can gener-

ate ATP under anaerobic conditions, glycolysis becomes an attractive alternate metabolic pathway for ATP generation in a hypoperfused myocardium with a limited supply of oxygen. Although the amount of energy produced by glycolysis may be adequate to maintain myocyte viability and preserve the electrochemical gradient across the cell membrane, it may not be sufficient to sustain contractile function. In hibernation, the adaptive response of the myocardium in the setting of prolonged resting hypoperfusion (reduced oxygen supply) is a reduction in myocardial contractile function (reduced oxygen demand), thereby preserving myocardial viability in the absence of clinically evident ischemia [21]



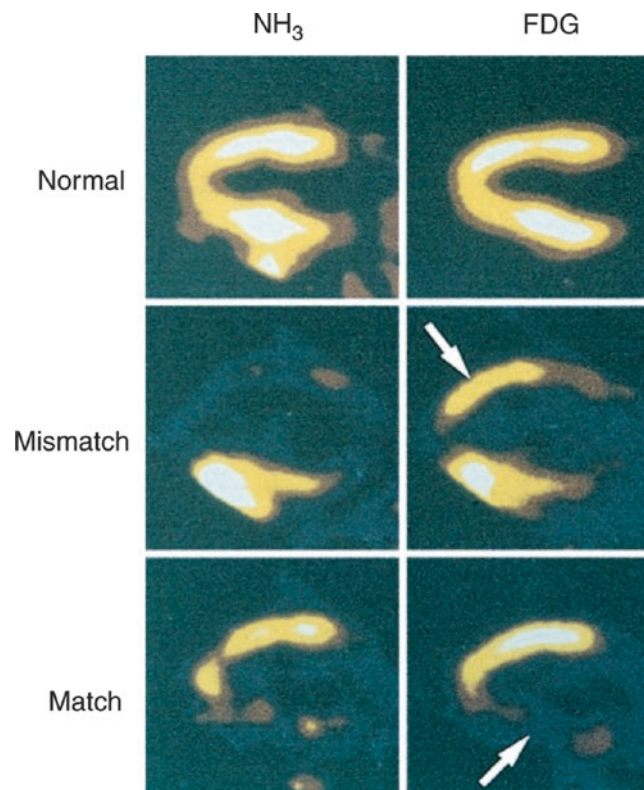


**Fig. 9.17** Myocardial perfusion/metabolism PET Scans. Patterns of normal, mismatch, and match under glucose loading. Preserved or increased myocardial glucose utilization in the setting of prolonged hypoperfusion at rest is termed a *mismatch pattern*. In the  $\text{NH}_3$  images, there is severely reduced blood flow in the anterior and lateral regions, but these have preserved metabolism in the FDG image (*arrow*), consistent with myocardial viability. Reduced or absent myocardial glucose utilization in hypoperfused myocardial regions is termed a *match pattern*. In the  $\text{NH}_3$  images, there is severely reduced blood flow in the

inferior region, which has absent myocardial metabolism in the FDG image (*arrow*), consistent with scarred myocardium. The application of such PET patterns in patients with chronic ischemic left ventricular dysfunction confers high positive and negative predictive accuracies for the recovery of regional function after revascularization, with an overall accuracy between 80% and 90% [22]. Clinically meaningful increases in global left ventricular function after revascularization are best attained if the extent of hibernating and stunned myocardium is at least 17–25% of the left ventricular mass [23]. (Courtesy of Dr. James Arrighi)



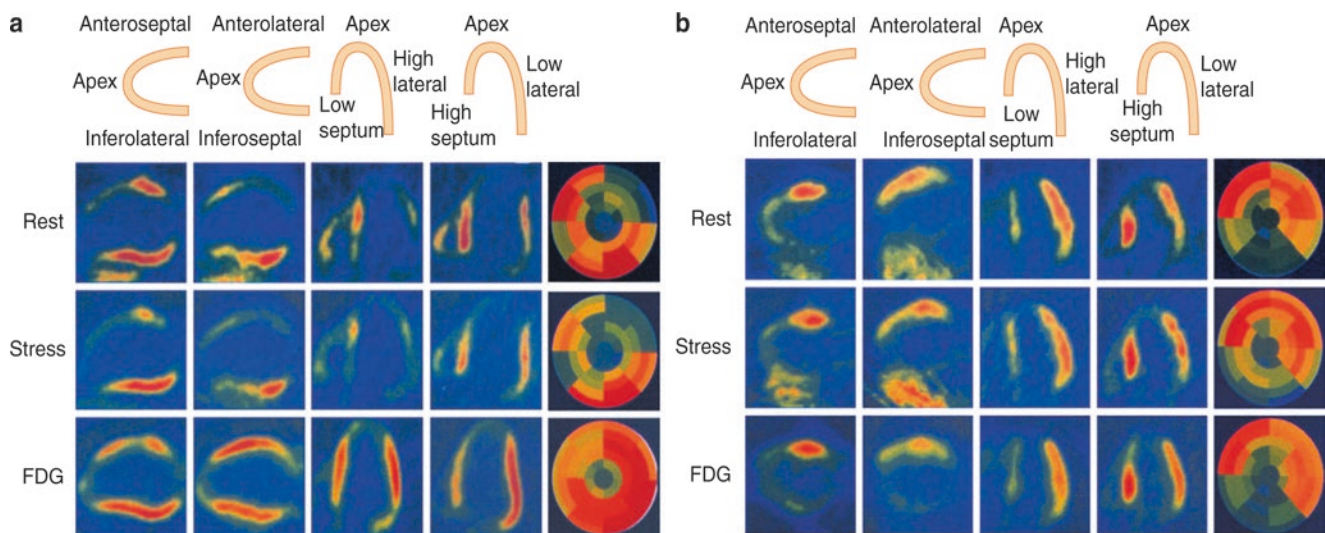


**Fig. 9.18** Examples of PET mismatch and match patterns. Increased FDG uptake in asynergic myocardial regions with reduced blood flow at rest (a mismatch pattern) has become a scintigraphic marker of hibernation. **(a)** A patient with a severely dilated left ventricle, diffuse hypokinesis, and apical dyskinesis (left ventricular ejection fraction [LVEF], 12%) had severe triple vessel disease. A coronary angiogram revealed a 100% occlusion of the proximal left anterior descending (LAD) coronary artery, D1, and D2; subtotal occlusion of the proximal right coronary artery (RCA); and a 90% OM1 occlusion. In this patient, four long-axis slices (two horizontal long-axis and two vertical long-axis images) encompassing the entire left ventricle along with corresponding bull's-eye images for rest and stress  $^{13}\text{N}$ -ammonia and FDG uptake are shown. Rest  $^{13}\text{N}$ -ammonia images show irreversible defects in the apical and anterolateral regions, with partial reversibility in the anterior and inferoseptal regions. Stress  $^{13}\text{N}$ -ammonia images show markedly decreased perfusion in the apical, anterior, anterolateral, and inferoseptal regions. However, FDG images acquired under glucose-loaded conditions show preserved or increased glucose utilization in all abnormally perfused myocardial regions at rest,

which is the scintigraphic hallmark of hibernation. In patients with chronic ischemic left ventricular dysfunction, rest and stress myocardial perfusion images alone may significantly underestimate the presence and extent of hibernating but viable myocardium. **(b)** Decreased or absent FDG uptake in asynergic myocardial regions with reduced blood flow at rest (a match pattern) represents scarred myocardium. A patient with previous coronary bypass surgery presented with a significantly dilated left ventricle, apical dyskinesis, septal and inferior akinesis (LVEF, 36%), and congestive heart failure. A coronary angiogram revealed severe native disease of all three vessels, patent left and right internal mammary grafts to the LAD and RCA, critical stenoses of the OM1 vein graft, and a patent OM2 vein graft. In this patient, rest and stress  $^{13}\text{N}$ -ammonia images show irreversible defects in the inferior, apical, and inferoseptal regions. FDG images acquired under glucose-loaded conditions show the absence of glucose utilization in all abnormally perfused myocardial regions at rest. Such asynergic myocardial regions, demonstrating matched reduction in perfusion and metabolism, represent scarred myocardium that is unlikely to recover function after revascularization

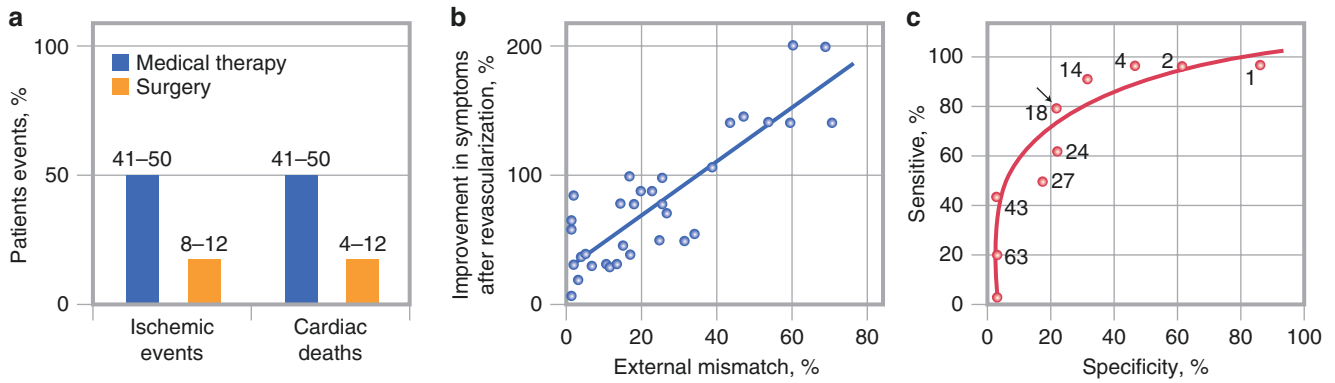


**Fig. 9.19** PET mismatch and prognosis. The prognostic significance of a perfusion–metabolism mismatch pattern in ischemic cardiomyopathy has been shown in a number of nonrandomized, retrospective studies with PET [24, 25]. (a) Patients with a perfusion–metabolism mismatch pattern who were treated surgically had lower ischemic event rates and fewer deaths than those treated with medical therapy. In contrast, patients with a perfusion–metabolism match pattern displayed no such difference in outcomes between surgical and medical management. Moreover, the patients with myocardial viability (a mismatch pattern) who underwent revascularization manifested a significant improvement in heart failure symptoms and exercise tolerance [26, 27]. (b) The relation between the anatomic extent of a perfusion metabolism

PET mismatch pattern (expressed as a percentage of the left ventricle) and the change in functional status after revascularization (expressed as a percent improvement from baseline) is shown. This scatterplot shows that the greatest improvement in heart failure symptoms occurs in patients with the largest mismatch defects in the quantitative analysis of PET images. (c) A receiver-operating characteristic curve is shown for the different anatomic extent of a perfusion–metabolism mismatch to predict a change (at least one grade) in functional status after revascularization. When the extent of PET mismatch involves 18% or more of the left ventricular mass, the sensitivity for predicting a change in the functional status after revascularization is 76%, and the specificity is 78% (the area under the fitted curve = 0.82)

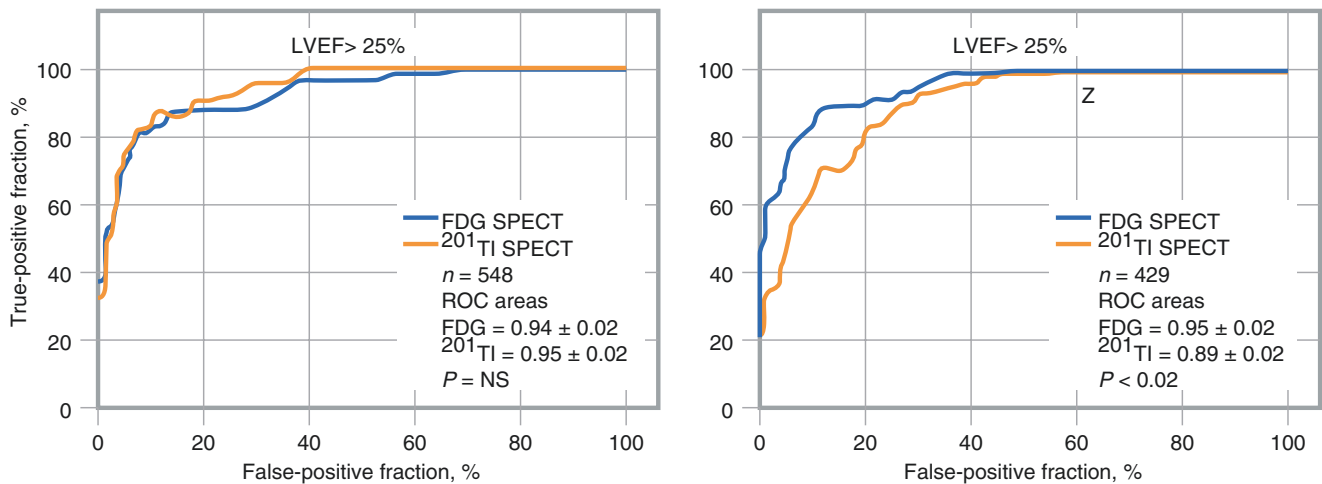


**Fig. 9.20** SPECT and PET with coronary artery disease. In patients with chronic coronary artery disease, differences between high-energy collimator SPECT and PET technologies and FDG and <sup>201</sup>Tl tracers are examined for their ability to differentiate between viable and nonviable myocardium. Shown are plots of receiver-operating characteristic (ROC) curves for <sup>201</sup>Tl and FDG SPECT to predict myocardial viability as defined by a 60% FDG PET threshold value for patients with left ventricular ejection fraction (LVEF) above 25% (left) and for patients

with LVEF 25% or less (right). The area under the ROC curve for FDG SPECT and <sup>201</sup>Tl SPECT are displayed for each panel. <sup>201</sup>Tl tends to underestimate the myocardial viability in patients with LVEF of 25% or less, but not in patients with LVEF above 25%. Of the severe asynergic regions, 73% of discordant regions between <sup>201</sup>Tl and FDG PET were located in the inferior segment, compared with only 27% of regions with concordance between <sup>201</sup>Tl and FDG PET ( $P < 0.001$ ) [28]

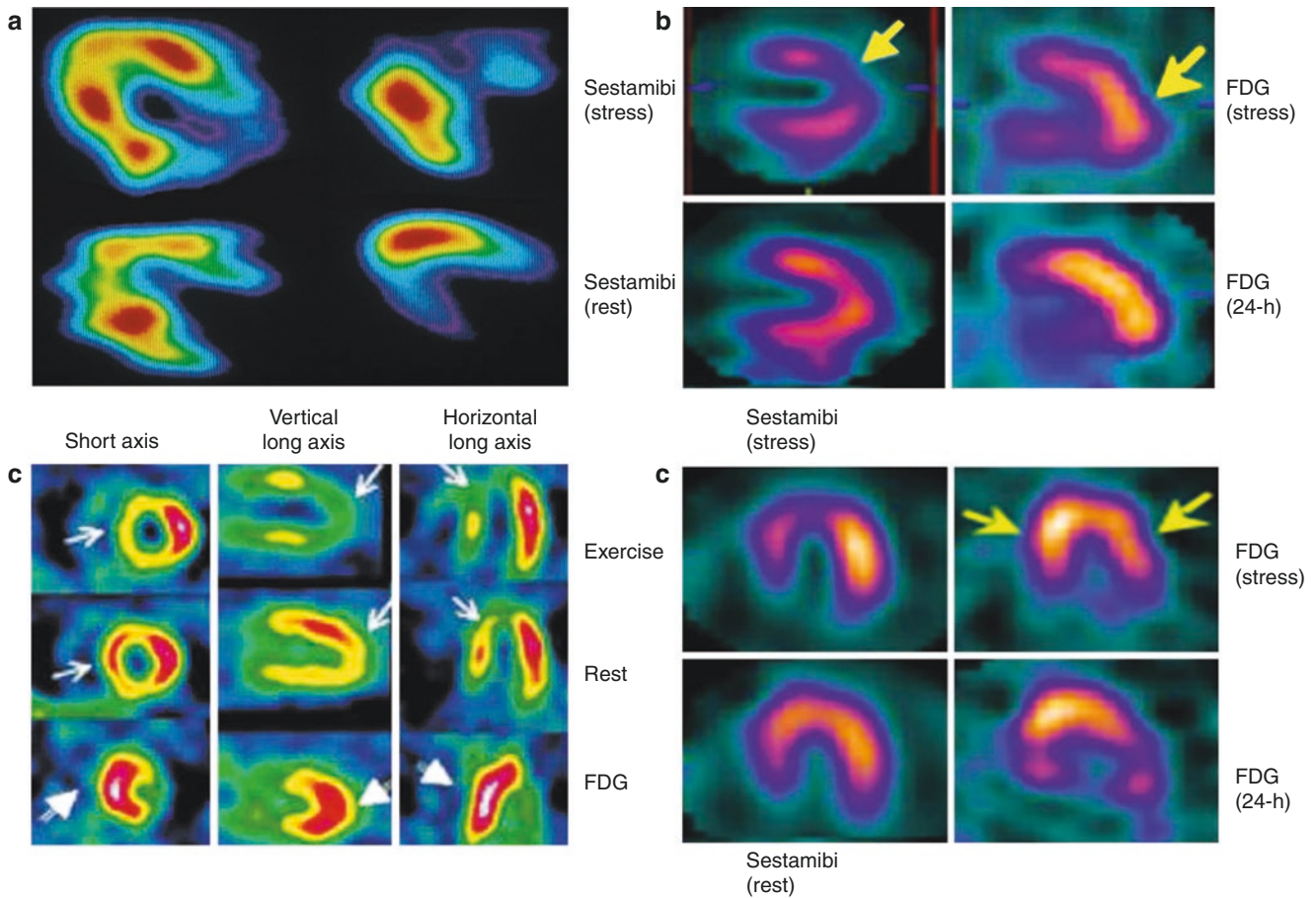


**Fig. 9.21** Metabolic alterations in postischemic myocardium in patients with angina. Physical exercise is probably the most common precipitating factor responsible for myocardial ischemia in patients with coronary artery disease manifested as angina and, most importantly, left ventricular dysfunction (mismatch of supply and demand). Although the recovery of such stress-induced left ventricular dysfunction is thought to occur within minutes after the termination of exercise, persistent contractile dysfunction has been observed in some patients up to 90 minutes after the termination of exercise, which has been attributed to stunned myocardium. (a) Transaxial rubidium-82 ( $^{82}\text{Rb}$ ) PET images reflecting myocardial blood flow at rest, during exercise, and after exercise are shown along with FDG images after exercise. At rest (*top left*), the distribution of myocardial blood flow is homogeneous in all myocardial regions. During exercise (*top right*), there are extensive blood flow abnormalities in the apical and anteroseptal regions that improve on the postexercise images (*bottom left*) and are comparable to the  $^{82}\text{Rb}$  rest image (*top left*). FDG was injected 8 minutes after the termination of exercise. The FDG image recorded 60 minutes after tracer injection (*bottom right*) shows metabolic alterations in the previously ischemic regions. (b) An example of perfusion/metabolism mismatch. Shown are simultaneous myocardial perfusion and metabolism imaging after dual intravenous injection of  $^{99\text{m}}\text{Tc}$ -sestamibi and FDG at peak exercise. Dual isotope simultaneous acquisition was carried out 40–60 minutes after the exercise study was completed. Rest  $^{99\text{m}}\text{Tc}$ -sestamibi imaging was carried out separately. In this patient with angina

and no prior myocardial infarction, there is evidence for extensive reversible perfusion defects in the anterior, septal, and apical regions (*white arrows*). The coronary angiogram showed 90% stenosis of the left anterior descending artery and 60% stenosis of the left circumflex coronary artery. The corresponding FDG image shows intense uptake in the regions with reversible sestamibi defects, reflecting the metabolic correlate of exercise-induced myocardial ischemia. (c, d) A persistent metabolic switch from fatty acid to glucose 24 hours after the resolution of transient myocardial ischemia on a treadmill is shown. Exercise and rest  $^{99\text{m}}\text{Tc}$ -sestamibi perfusion (*left*) and FDG (*right*) images are shown of a 71-year-old man with exertional angina in the vertical (c) and horizontal long-axis (d) views. Reversible perfusion abnormalities involving the anterior, apical, and septal regions (*yellow arrows*) are shown on sestamibi images with intense FDG uptake in the corresponding reversible anterior and septal regions. Rest FDG PET images acquired after the reinjection of FDG, 24 hours after the treadmill study (without interim exercise), shows persistent increased metabolic activity in the regions of the exercise-induced ischemia. This patient had 90% stenosis of the left anterior descending coronary artery. Thus, metabolism plays a critical role in sustaining myocellular viability by adapting quickly to the ischemic injury response, albeit with a prolonged recovery phase, with the recovery of metabolism lagging behind perfusion for 24 hours or more [29–32]. (a, From Camici et al. [30], with permission from Wolters Kluwer)



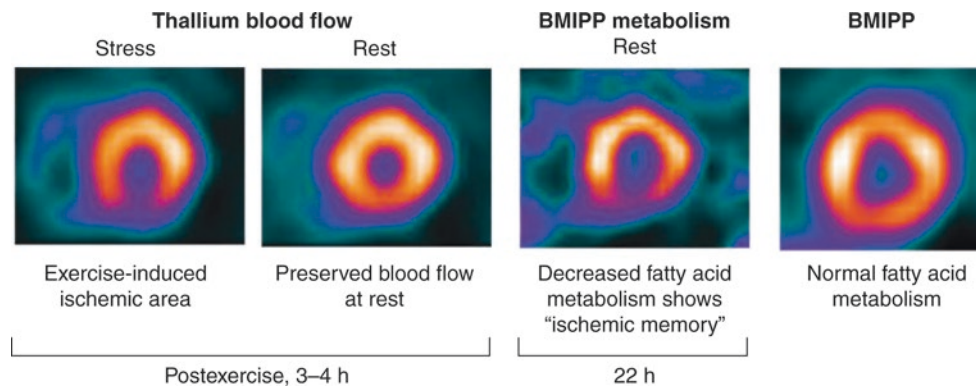


**Fig. 9.22** SPECT images showing delayed recovery of regional fatty acid metabolism after transient exercise-induced ischemia, termed *ischemic memory*. Representative stress and rest reinjection short-axis thallium tomograms demonstrate a reversible inferior defect consistent with exercise-induced myocardial ischemia. A BMIPP-labeled tomogram injected and acquired at rest 22 hours after exercise-induced isch-

emia shows persistent metabolic abnormality in the inferior region despite complete recovery of the regional perfusion at rest, as evidenced by the thallium reinjection image. For comparison, the tomogram on the *far right* shows retention of BMIPP in the heart of a normal adult [33, 34]

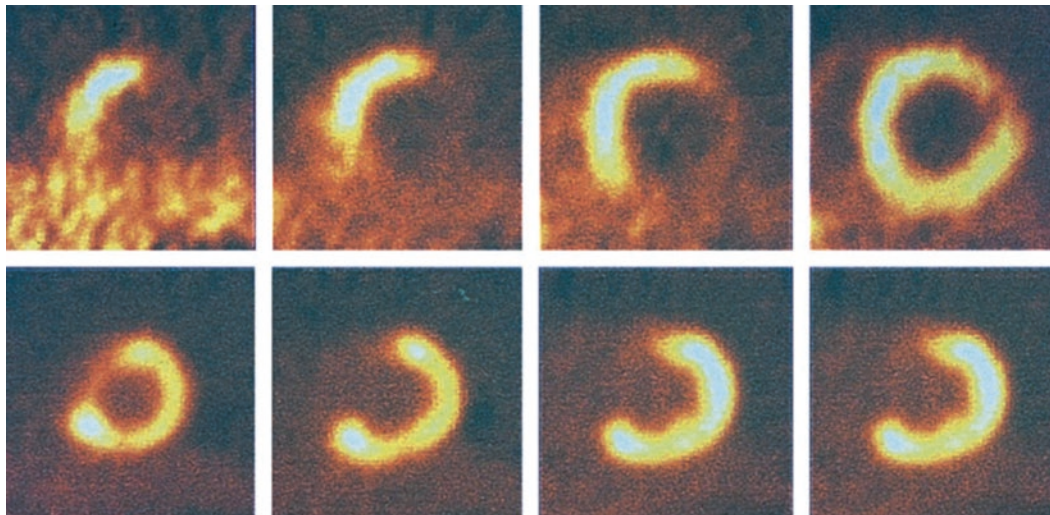


**Fig. 9.23** PET scans demonstrating perfusion-metabolism mismatch (reduced blood flow with preserved or enhanced FDG uptake) in a patient with chronic ischemic left ventricular dysfunction and heart failure symptoms. The principle of using a metabolic tracer, such as FDG, is based on the concept that viable myocytes in hypoperfused and dysfunctional regions are metabolically active, whereas scarred or fibrotic tissue is metabolically inactive. Although fatty acids are the primary source of myocardial energy production in the fasting state, in the setting of reduced oxygen supply (a consequence of hypoperfusion at rest), the myocytes compensate for the loss of oxidative potential by shifting toward greater glucose utilization to generate high-energy phosphates. Thus, in chronic ischemia, aerobic metabolism is slowed

while the anaerobic metabolism is accelerated, a reversal of the well-known Pasteur effect [35]. Such increased FDG uptake (anaerobic metabolism) in asynergic myocardial regions with reduced blood flow at rest has become a scintigraphic marker of hibernation. *Top row:* Short-axis [ $^{13}\text{N}$ ]-ammonia scans demonstrate large lateral and inferior perfusion defects at rest. *Bottom row:* The corresponding FDG images acquired under fasting conditions demonstrate that FDG metabolic activity is preserved in the lateral and inferior regions (mismatch pattern). On the other hand, the lack of FDG metabolic activity in the anterior and septal regions reflects the utilization of fatty acid rather than glucose as the primary fuel in such normally perfused myocardial regions

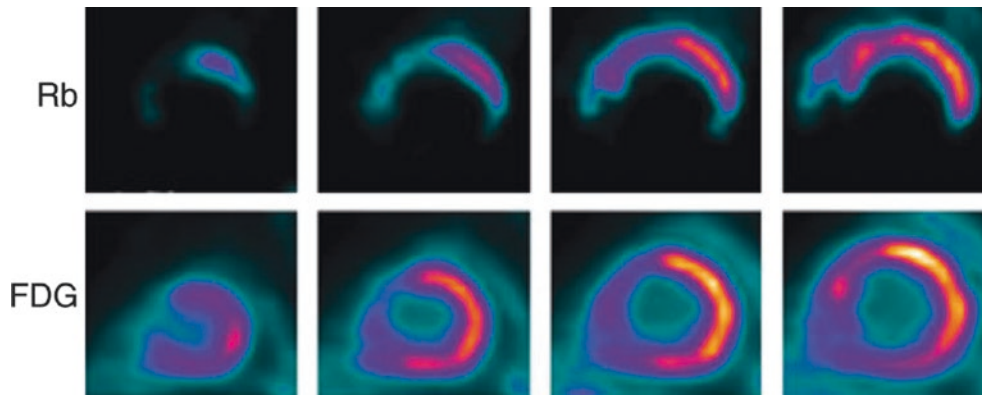


**Fig. 9.24** PET scan showing a perfusion-metabolism mismatch in hibernating heart tissue as an example of preserved cardiometabolic reserve. *Top*: Rubidium (Rb)-82-labeled positron emission tomography in the short-axis view shows markedly decreased perfusion defects in the apical, inferior, inferolateral, and septal regions of the left ventricle at rest, which extends from distal to basal slices. *Bottom*: Images

acquired under glucose-loaded conditions, labeled with FDG, show a perfusion-metabolism mismatch pattern (the scintigraphic hallmark of hibernation) in all abnormally perfused myocardial regions at rest. An exception is the anteroseptal region, which demonstrates a matched perfusion-metabolism pattern (compatible with scarred myocardium). Adapted from Taegtmeier & Dilzian with permission [33]

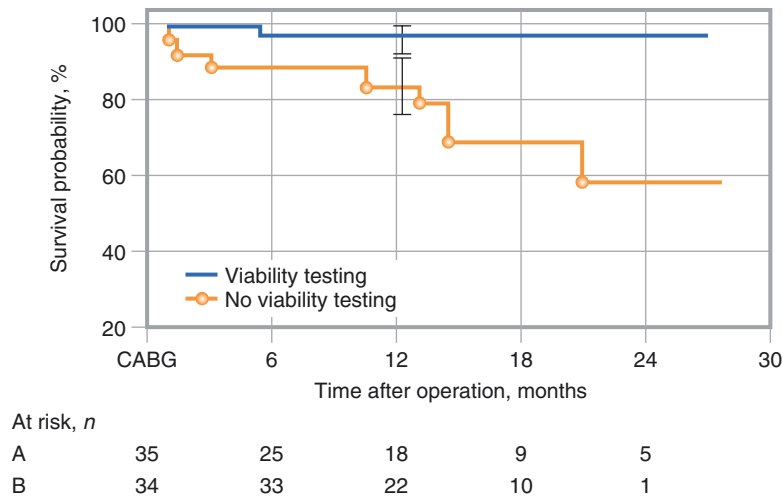


**Fig. 9.25** Myocardial viability testing prior to surgical revascularization. The determination of myocardial viability evaluation in patients with coronary artery disease and severe left ventricular dysfunction before referral to coronary artery revascularization affects the clinical outcome with respect to both in-hospital mortality and the 1-year survival rate. In this retrospective study, the perioperative and postoperative event-free survival rate was significantly lower in patients who were referred to revascularization on the basis of clinical presentation

and angiographic data but without viability testing (group A) compared with those who were selected according to the extent of viable tissue determined by positron emission tomography (group B) in addition to clinical presentation and angiographic data. There were four in-hospital deaths (11.4%) in group A and none in group B ( $P=0.04$ ). Moreover, after 12 months, the survival rate was 79% in group A and 97% in group B ( $P=0.01$ ) [27]. CABG coronary artery bypass graft

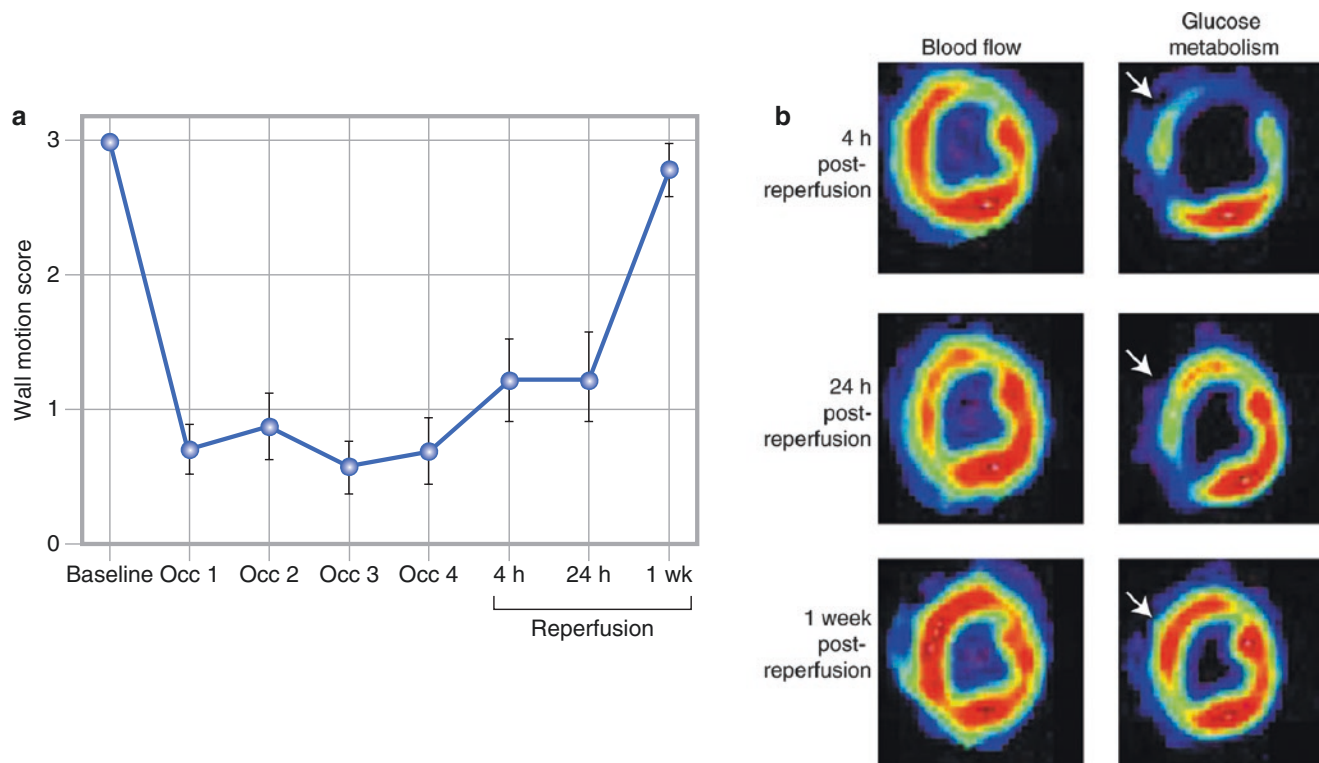


**Fig. 9.26** Alterations in contractile function, regional blood flow, and glucose metabolism in myocardial stunning. **(a)** Anesthetized dogs underwent four sequential 5-minute intervals of balloon left anterior descending coronary artery occlusion (Occ), each separated by 5 minutes of reperfusion. Regional blood flow, metabolism, and function were evaluated 4 hours, 24 hours, and 1 week after reperfusion. The regional wall motion was severely depressed in the anterior and antero-septal regions after the four cycles of ischemia, remained impaired 24 hours after reperfusion, but normalized 1 week later, which is consistent with myocardial stunning. **(b)** Representative mid-short-axis PET images of [ $^{13}\text{N}$ ]-ammonia (blood flow) and FDG (glucose metabolism) were obtained 4 hours, 24 hours, and 1 week after reperfusion. In the images obtained 4 hours after reperfusion, the regional myocardial blood flow is near normal in the anterior and antero-septal region,

whereas glucose utilization is severely reduced (*arrow*). In images obtained 24 hours after reperfusion, the regional myocardial blood flow remains near normal, and there is evidence of a partial recovery in glucose utilization in the anterior and antero-septal regions (*arrow*). In the images obtained 1 week after reperfusion, there is complete recovery of glucose utilization in the regions of stunned myocardium, which appear homogeneous with remote myocardial regions (*arrow*). These findings suggest that, in repetitive myocardial stunning, a unique metabolic adaptation occurs (abnormal glucose utilization despite the restoration of regional blood flow) that is different from the adaptation typically described in clinical and experimental models of myocardial hibernation (preserved or enhanced glucose utilization in a region with decreased regional blood flow) [36]



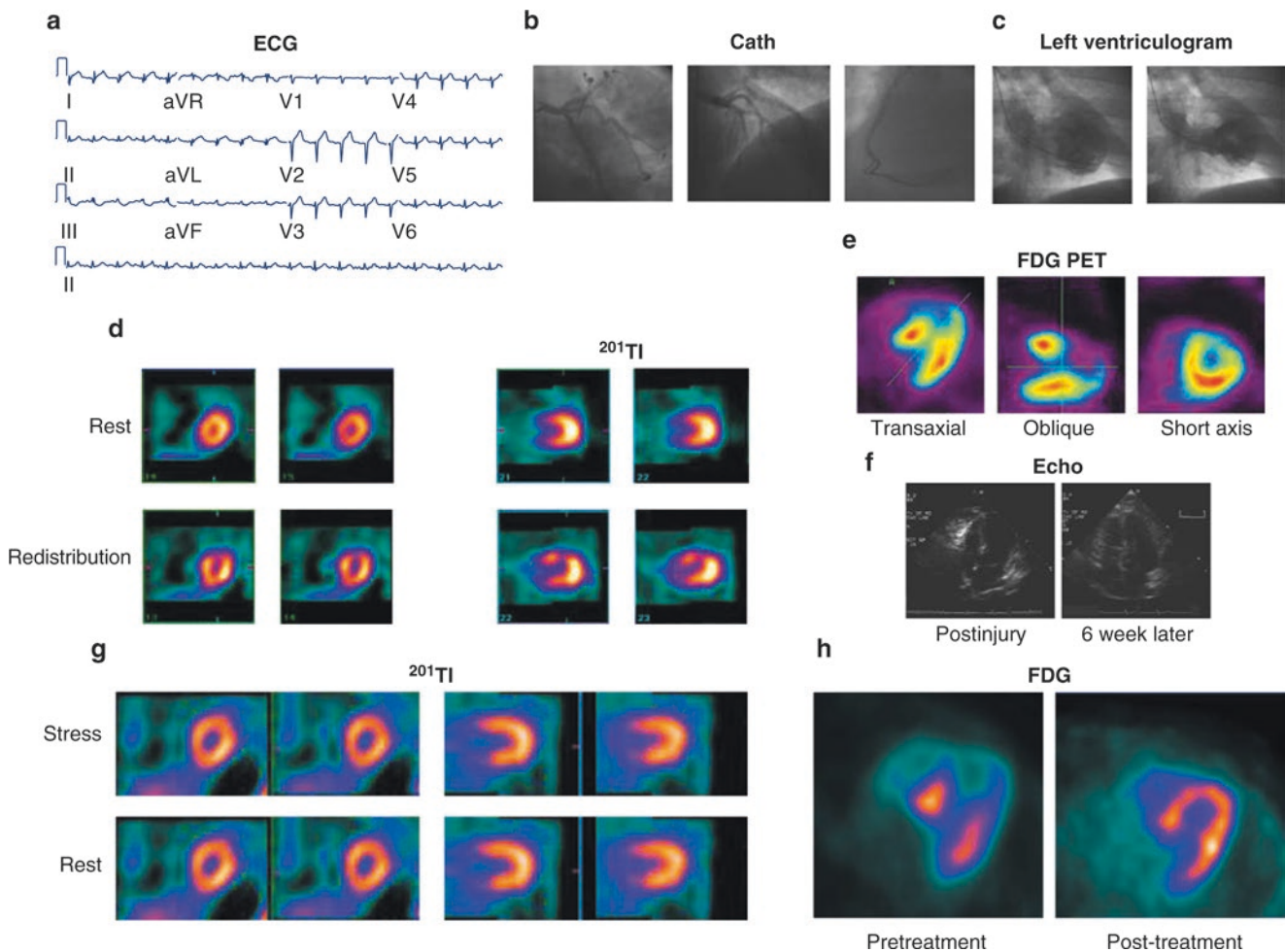


**Fig. 9.27** Scintigraphic pattern of stunned myocardium. A patient with end-stage liver disease and a family history of coronary artery disease presents to the emergency department with 1 hour of new-onset chest pain. The electrocardiogram (ECG) pattern (a) is consistent with acute ST segment elevation myocardial infarction. The coronary angiogram (b) shows normal-appearing, insignificant coronary artery disease. The left ventriculogram (c) shows extensive left ventricular apical, anterior, and anterolateral akinesis, with a calculated ejection fraction of 30% (*left panel*, diastole; *right panel*, systole). The patient had a mild rise in cardiac enzymes (troponin, 1.5; serum creatine kinase, 76; MB, 5; %MB, 6.6), which is indicative of myocardial injury. Rest-redistribution  $^{201}\text{Tl}$  SPECT images acquired within 1 week after the onset of chest pain (d) show normal perfusion at rest (*top row*), with evidence for a rapid  $^{201}\text{Tl}$  washout in the anterior region in  $^{201}\text{Tl}$  redistribution images (*bottom row*), which is consistent with reverse redistribution. FDG PET images acquired within days after the thallium study (e) show severely impaired glucose utilization in the anterior and apical regions. These scintigraphic findings (abnormal glucose utilization or retention of  $^{201}\text{Tl}$  in redistribution images despite normal regional blood flow on rest

$^{201}\text{Tl}$ ) are compatible with stunned myocardium. Repeat echocardiography (f), myocardial perfusion SPECT (g), and FDG PET studies (h) approximately 6 weeks after the acute ischemic injury show a complete resolution of the extensive left ventricular apical akinesis (f) with homogeneous and normal glucose utilization in all myocardial regions (h) and no evidence of myocardial ischemia (g). A similar presentation of transient left ventricular apical ballooning by echocardiography, termed *tako-tsubo*, has been observed in critically ill patients who are being admitted to the medical intensive care unit for noncardiac medical disorders. Elevated serum creatine kinase has been described in up to 50% of patients with ventricular apical ballooning, with a subset of these patients also exhibiting ECG evidence of Q-wave and/or ST-segment displacement. Although possible triggering factors have been suggested in the literature, the underlying pathophysiology for the left ventricular dysfunction and apical ballooning has not been elucidated. The transient nature of the apical dysfunction in a subset of patients could be attributed to transient ischemic injury and myocardial stunning. Cath catheterization, Echo echocardiogram. (Courtesy of Mark Kelemen and Vasken Dilsizian)

Similarly, the ability of PET to define a myocardial scar is of significant interest to electrophysiologists. A myocardial scar usually acts as the substrate for reentrant ventricular tachycardia (VT) and is present in the majority of patients with ischemic and nonischemic cardiomyopathy. During reentrant VT, an electrical wave front enters and traverses the myocardial scar via a network of electrically conducting channels. After exiting the scar, it depolarizes the rest of the ventricle and returns to the original entry site, repeating the cycle. This concept of entry sites, slowly conducting channels, and exit sites has been successfully validated in post-myocardial infarction patients during clinical electrophysiologic studies. The current “gold standard” of defining a myocardial scar is based on endocardial bipolar voltage recordings using a three-dimensional (3D) mapping system with a roving mapping catheter. Accordingly, regions with greater than 1.5 mV are classified as normal myocardium, 0.5–1.5 mV as abnormal myocardium, and less than 0.5 mV as scarred myocardium. Different from delayed-enhanced MRI and CT, which provide a morphologic substrate assessment, PET allows a metabolic characterization of the myocardial scar and its border zone. Current software developments are aimed at exporting this detailed 3D imaging information into the actual ablation procedure to provide anatomic guidance for patients with recurrent episodes of VT. In a recent study of patients undergoing VT ablation, a good correlation was found between PET-derived metabolic scar maps and endocardial voltage ( $r = 0.89$ ,  $P < 0.05$ ). The scar size, location, and border zone accurately predicted high-resolution voltage map findings ( $r = 0.87$ ,  $P < 0.05$ ). Moreover, PET/CT maps correctly predicted a nontransmural epicardial scar that was confirmed with epicardial mapping despite a normal endocardial map [37]. Figure 9.28 illustrates a fusion of CT and PET FDG images that could be used to guide VT ablation therapy.

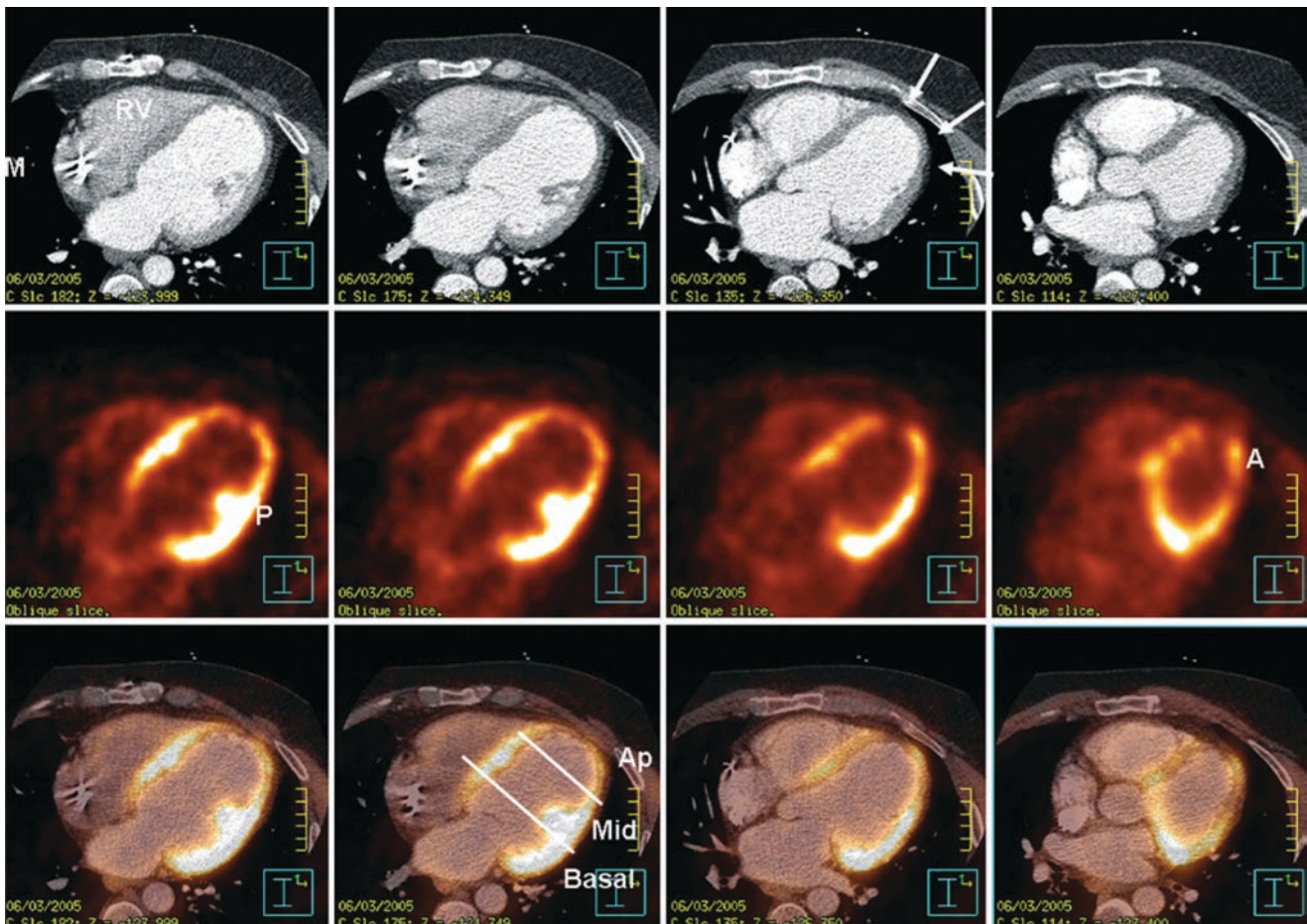


**Fig. 9.28** A fusion of PET FDG and CT images for use in PET-guided ventricular tachycardia ablation therapy. *Top row:* Contrast-enhanced CT demonstrates all cardiac chambers, including the right ventricle (RV), left ventricle (LV), and a metal artifact (M) of an implantable cardioverter defibrillator lead in the right atrium. Significant wall thinning (arrows) is noted in the apical and lateral LV walls, which is consistent with myocardial infarction. *Middle row:* A matching decrease in signal intensity in apical and lateral wall segments is observed in PET

images. A preserved metabolism of papillary muscle (P) is seen, with areas of preserved metabolic activity (A) within the lateral wall, which appears to be uniformly thinned on the CT images. *Bottom row:* PET images are fused with corresponding CT datasets to allow visualization of metabolic and anatomic datasets. The LV wall is divided into the apical (Ap), mid, and basal sections for conventional 17-segment analysis. Adapted from Dickfeld et al. with permission [37]

Figures 9.29 and 9.30 demonstrate metabolic alterations in chronic kidney disease (CKD) and renal failure. The detection of early preclinical myocardial metabolic alterations in CKD can be limited. Although the distribution of FDG uptake may visually appear homogeneous throughout the left ventricular myocardium, absolute myocardial glucose utilization may be abnormal in these patients.

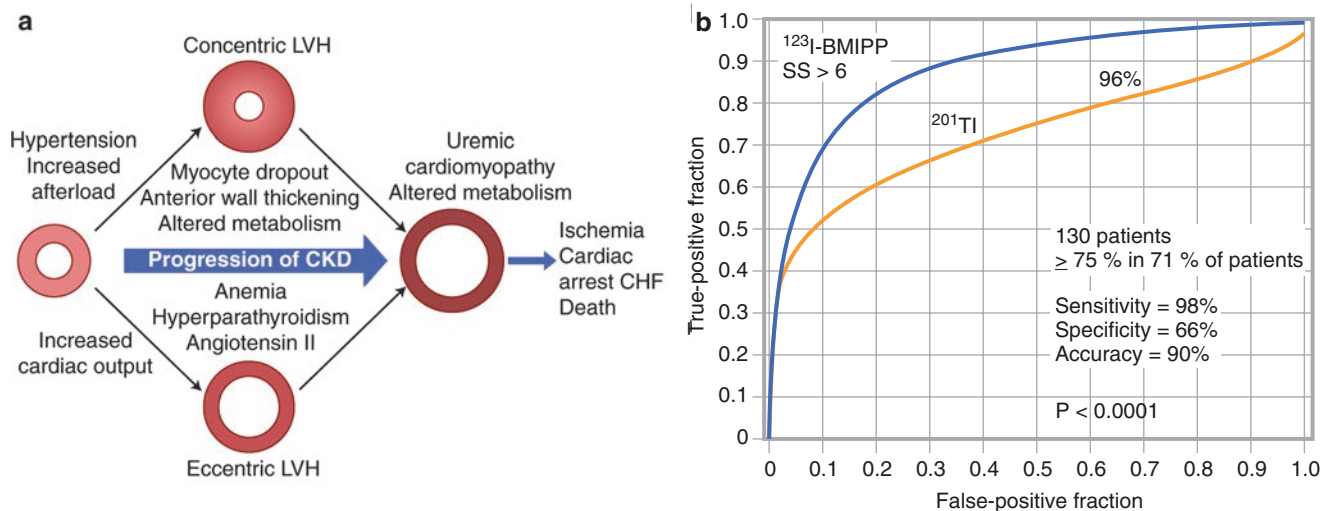


**Fig. 9.29** Metabolic alterations in renal failure. **(a)** Concurrent pathogenic factors contribute to the development of uremic cardiomyopathy and an altered metabolism with declining kidney function in chronic kidney disease (CKD). Though myocardial infarction and ischemic heart disease account for a significant portion of patients with heart failure and left ventricular remodeling, several sequelae of renal failure that accrue with the loss of renal function can also contribute to left ventricular remodeling, termed *uremic cardiomyopathy*. The United States Renal Data System has reported nearly identical rates of myocardial infarction and cardiac death in dialysis patients and an approximately tenfold higher rate of heart failure in the same population [38]. The common occurrence of heart failure in the dialysis population is thought to be related to left ventricular hypertrophy (LVH), which occurs frequently in patients with CKD. Although hypertension is common among patients with kidney disease, several investigators have suggested that elevated blood pressure becomes increasingly volume-dependent, with a concomitant increase in arterial stiffening, activation of neurohormones, and endothelial dysfunction as renal function declines. Individuals with CKD, therefore, are faced with both pressure- and volume-overload states contributing to the development of left ventricular remodeling and heart failure. The cardiomyopathy typical of CKD and the associated uremia is thought to lead to a myocyte-capillary mismatch, with a diminished vascular supply relative to the number and volume of functioning myocytes [39]. The oxygen-poor milieu will lead to diffuse myocardial ischemia with an anticipated decline in aerobic myocardial fatty acid utilization and a shift to anaerobic metabolism, with increased uptake of glucose as the principal energy-providing substrate [40, 41]. The shift from a predominance of aerobic (fatty acid) to anaerobic (glucose) metabolism appears to account for a significant portion of the excessive cardiovascular morbidity and mortality observed across all stages of kidney disease. **(b)** In a prospective study of 130 asymptomatic patients with end-stage renal disease (ESRD) who were undergoing hemodialysis, the prevalence of coronary artery disease was assessed by performing dual isotope thal-

lium and  $\beta$ -methyl-p-[ $^{123}\text{I}$ ]-iodophenyl-pentadecanoic acid (BMIPP) SPECT imaging at rest, followed by coronary angiography [42, 43]. Significant coronary artery luminal narrowing (>75%) was present in 71.5% (93 of 130) of the ESRD patients, with an additional five patients exhibiting a coronary vasospasm. When a reduced myocardial metabolism with BMIPP (summed score of 6 or more) was used to define an abnormal scan, the BMIPP SPECT showed 98% sensitivity, 66% specificity, and 90% accuracy for detecting coronary artery disease at rest [42]. **(c)** In a subsequent publication by the same investigators, the prognostic significance of a reduced myocardial metabolism with BMIPP in conjunction with perfusion abnormalities assessed with thallium in ESRD patients was examined [40]. Among 318 prospectively enrolled asymptomatic hemodialysis patients without prior myocardial infarction, 50 (16%) died of cardiac events during a mean follow-up period of  $3.6 \pm 1.0$  years. Kaplan-Meier survival estimates showed a 61% event-free survival at 3 years among patients with summed BMIPP score of 12 or more and a 98% score in patients with a summed BMIPP score below 12, with a graded relationship between survival and the severity of the summed BMIPP score. **(d)** When BMIPP uptake (metabolism) was assessed in relation to regional thallium uptake (perfusion), indicating myocardial ischemia, the sensitivity of the metabolism-perfusion mismatch for predicting cardiac death was 86%, and the specificity was 88%. Kaplan-Meier survival estimates showed 53% event-free survival at 3 years among patients with a BMIPP-thallium mismatch score of 7 or more, and 96% in patients with a BMIPP-thallium mismatch score below 7. These findings support the assertion that altered cardiac metabolism (indicating silent myocardial ischemia) is highly prevalent in ESRD patients and can identify the subgroup of patients who are at high risk for cardiac death. The shift from a predominance of aerobic (fatty acid) to anaerobic (glucose) metabolism appears to account for a significant portion of the excessive cardiovascular morbidity and mortality observed across all stages of kidney disease. CHF congestive heart failure



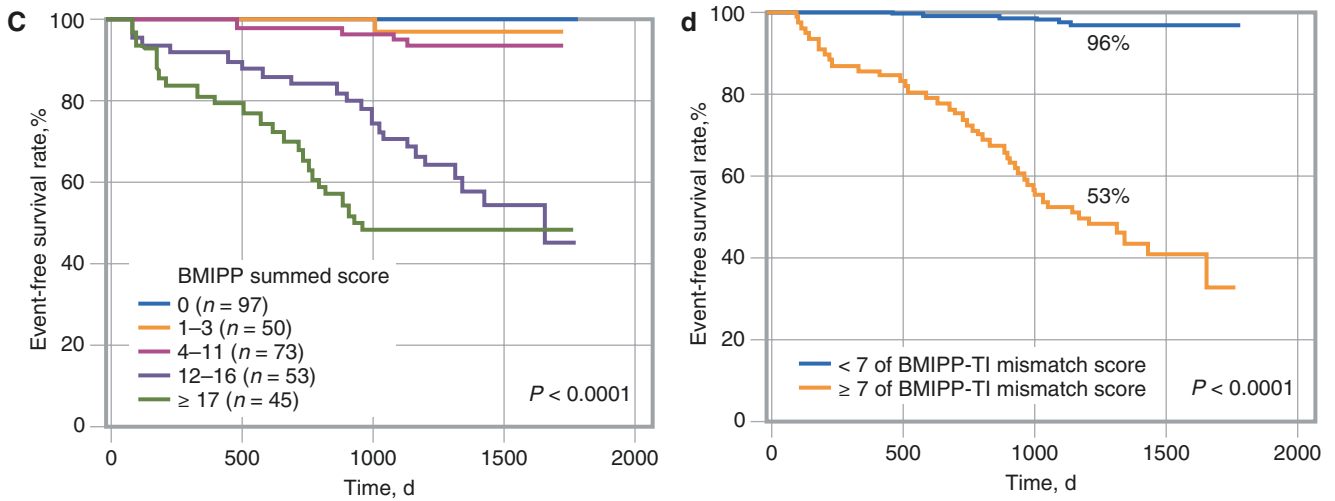
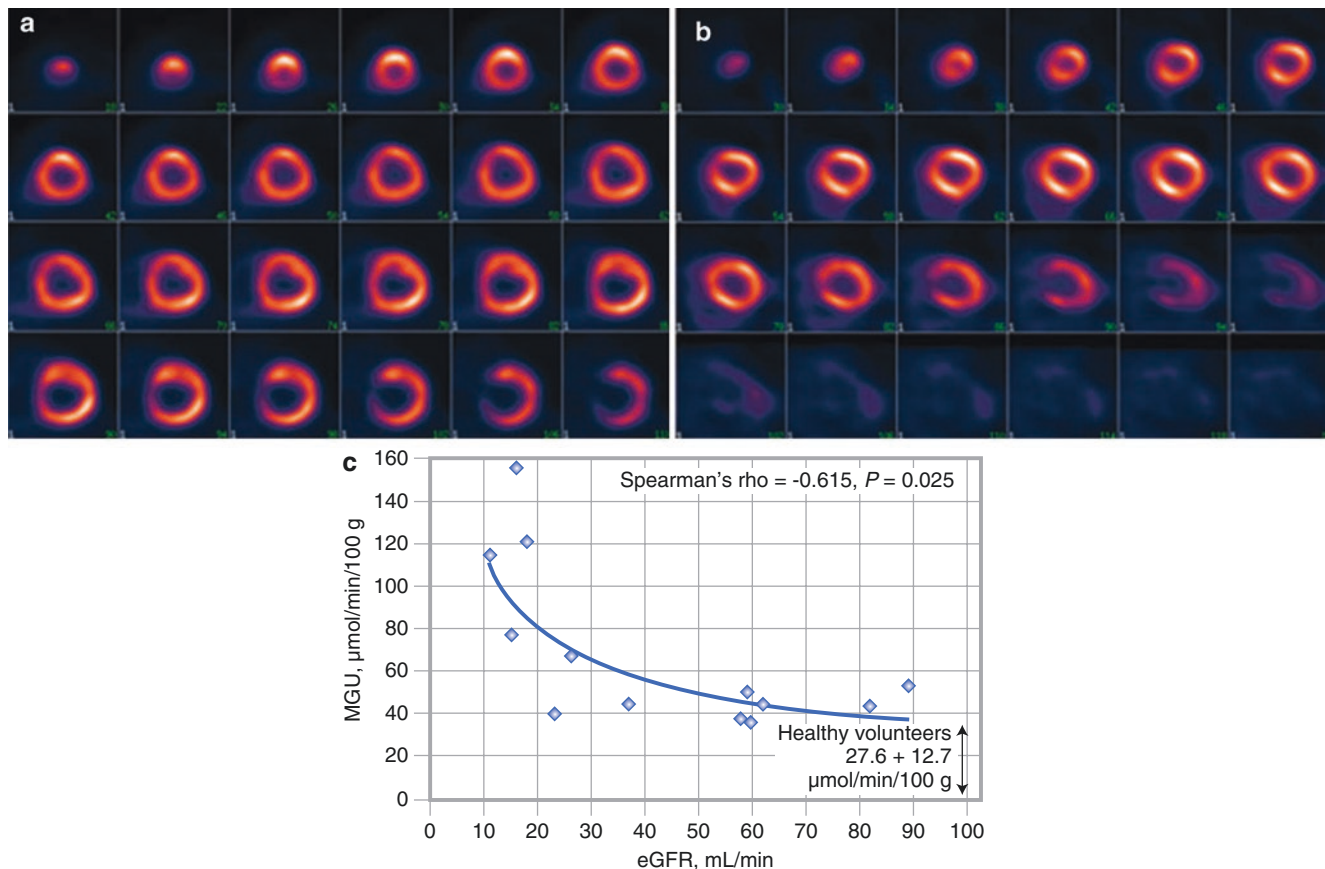


Fig. 9.29 (continued)



**Fig. 9.30** Preclinical myocardial metabolic alterations in chronic kidney disease (CKD). Examples of myocardial FDG distribution in CKD patients exhibiting no visually discernible regional defects are shown: (a), A CKD patient shows a dilated left ventricular cavity and concentric hypertrophy; (b), A CKD patient shows a normal left ventricular cavity size without hypertrophy. A quantitative assessment with PET may identify alterations in the whole myocardium glucose uptake (MGU), measured in  $\mu\text{mol}/\text{min}/100\text{ g}$  of myocardial tissue in the heart before clinical, functional, and prognostic consequences ensue. The feasibility of employing quantitative MGU with PET to gain additional insight into the alterations of myocardial metabolism in CKD patients was recently studied [44]. (c) A scatter plot of estimated glomerular

filtration rate (eGFR, mL/min/1.73 m<sup>2</sup>) versus MGU ( $\mu\text{mol}/\text{min}/100\text{ g}$ ) is shown, as measured by an [<sup>18</sup>F]-FDG PET scan in CKD. There is a significant inverse correlation between myocardial glucose uptake and renal function, assessed by eGFR. Of great interest was the degree to which myocardial glucose uptake increased with declining renal function across individuals. This increase was particularly notable among the subgroup with significant impairment in renal function, with Stage III or greater CKD. The relationship between myocardial glucose uptake and eGFR could not be ascribed to demographic factors or cardiac workload. Thus, [<sup>18</sup>F]-FDG PET may be an effective tool to investigate preclinical changes in the myocardial metabolism in CKD

Finally, Fig. 9.31 demonstrates bone marrow cell homing, an example of the new fields of metabolomics and stem-cell imaging, which may offer new tools of metabolic imaging for the diagnosis and treatment of myocardial diseases.

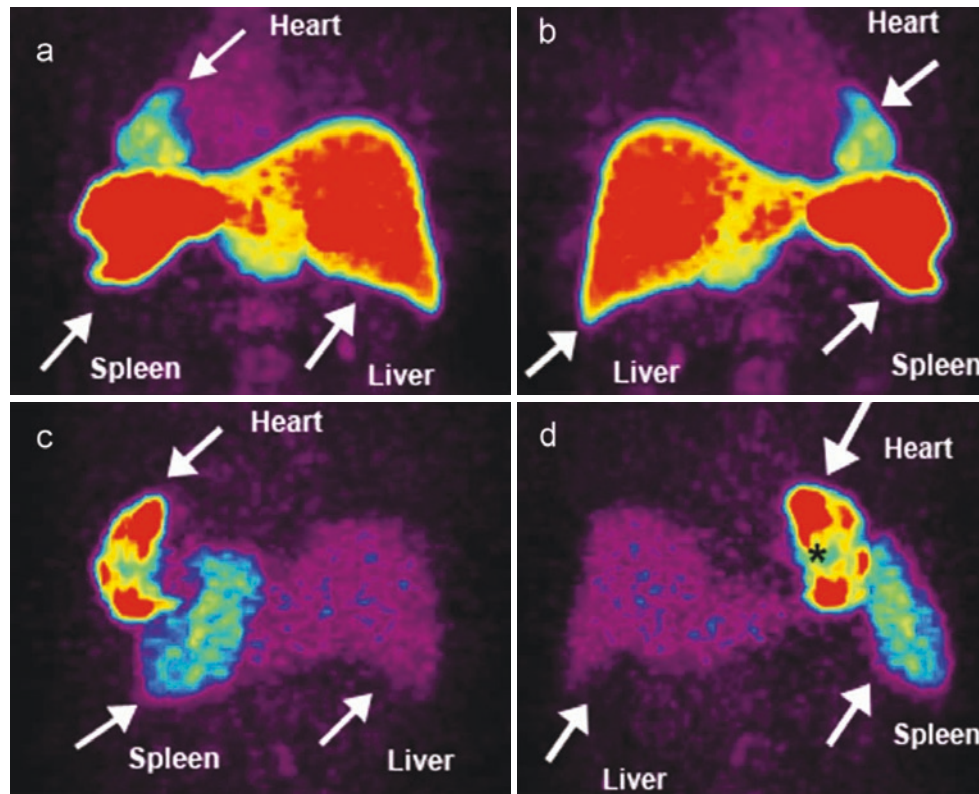


**Fig. 9.31** Myocardial homing and biodistribution of FDG-labeled bone marrow cells [45]. Shown are the left posterior oblique (a) and left anterior oblique (b) views of the chest and upper abdomen of the patient taken 65 minutes after the transfer of  $^{18}\text{F}$ -FDG-labeled, unselected bone marrow cells into the left circumflex coronary artery, and the left posterior oblique (c) and left anterior oblique (d) views of the chest and upper abdomen of another patient taken 70 minutes after the transfer of  $^{18}\text{F}$ -FDG-labeled, CD34-enriched bone marrow cells into the left anterior descending coronary artery. In both patient examples, bone marrow cell homing is detectable in the heart (infarct center and border zone), liver, and spleen. CD34<sup>+</sup> cell homing is most prominent in infarct border zone, but not infarct center (*asterisk*). Our current knowledge of the dynamics of intermediary metabolism remains fragmented and poorly

integrated into the biology of the cell. The new and powerful tools of systems biology give a fresh approach to the diagnosis and treatment of different forms of heart disease. A case in point is the field of metabolomics. In analogy to the genome, transcriptome, and proteome, the metabolome has been defined as the total set of low-molecular-weight metabolites. The techniques of metabolomics allow us to analyze changes in the metabolome in a given system. A major advantage of this metabolic profiling is the comparatively small number of possible targets. The new fields of metabolomics and stem-cell imaging offer challenges to both the experimental biologist and the clinical cardiologist to refine the tools of metabolic imaging for the diagnosis and treatment of myocardial diseases. (Courtesy of Kai C. Wollert)

## References

1. Taegtmeier H, Young ME, Lopaschuk GD, Abel ED, Brunengraber H, Darley-Usmar V, et al. American Heart Association Council on basic cardiovascular sciences. Assessing cardiac metabolism: a scientific statement from the American Heart Association. *Circ Res*. 2016;118:1659–701.
2. Kundu B, Zhong M, Sen S, Davogusto G, Keller S, Taegtmeier H. Remodeling of glucose metabolism precedes pressure overload-induced left ventricular hypertrophy: review of a hypothesis. *Cardiology*. 2015;130:211–20.
3. Taegtmeier H, Golfman L, Sharma S, Razeghi P, van Arsdall M. Linking gene expression to function: metabolic flexibility in the normal and diseased heart. *Ann N Y Acad Sci*. 2004;1015:202–13.
4. Taegtmeier H, Lam T, Davogusto G. Cardiac metabolism in perspective. *Compr Physiol*. 2016;6:1675–99.
5. Davogusto G, Taegtmeier H. The changing landscape of cardiac metabolism. *J Mol Cell Cardiol*. 2015;84:129–32.
6. Taegtmeier H, Hems R, Krebs HA. Utilization of energy-providing substrates in the isolated working rat heart. *Biochem J*. 1980;186:701–11.
7. Osterholt M, Sen S, Dilsizian V, Taegtmeier H. Targeted metabolic imaging to improve the management of heart disease. *JACC Cardiovasc Imaging*. 2012;5:214–26.
8. Depre C, Young ME, Ying J, Ahuja HS, Han Q, Garza N, et al. Streptozotocin-induced changes in cardiac gene expression in the absence of severe contractile dysfunction. *J Mol Cell Cardiol*. 2000;32:985–96.
9. Goodwin GW, Taylor CS, Taegtmeier H. Regulation of energy metabolism of the heart during acute increase in heart work. *J Biol Chem*. 1998;273:29530–9.
10. Nguyen VT, Mossberg KA, Tewson TJ, Wong WH, Rowe RW, Coleman GM, Taegtmeier H. Temporal analysis of myocardial glucose metabolism by 2-[18F]fluoro-2-deoxy-D-glucose. *Am J Phys*. 1990;259:H1022–31.
11. Sharma S, Adroque JV, Golfman L, Uray I, Lemm J, Youker K, et al. Intramyocardial lipid accumulation in the failing human heart resembles the lipotoxic rat heart. *FASEB J*. 2004;18:1692–700.
12. Taegtmeier H, McNulty P, Young ME. Adaptation and maladaptation of the heart in diabetes: part I: general concepts. *Circulation*. 2002;105:1727–33.
13. Depre C, Shipley GL, Chen W, Han Q, Doenst T, Moore ML, et al. Unloaded heart in vivo replicates fetal gene expression of cardiac hypertrophy. *Nat Med*. 1998;4:1269–75.
14. Dewald O, Sharma S, Adroque J, Salazar R, Duerr GD, Crapo JD, et al. Downregulation of peroxisome proliferator-activated receptor- $\alpha$  gene expression in a mouse model of ischemic cardiomyopathy is dependent on reactive oxygen species and prevents lipotoxicity. *Circulation*. 2005;112:407–15.
15. Feinendegen LE. Myocardial imaging of lipid metabolism with labeled fatty acids. In: Dilsizian V, editor. *Myocardial viability: a clinical and scientific treatise*. Armonk: Futura; 2000. p. 349–89.
16. Messina SA, Aras O, Dilsizian V. Delayed recovery of fatty acid metabolism after transient myocardial ischemia: a potential imaging target for “ischemic memory”. *Curr Cardiol Rep*. 2007;9:159–65.
17. Gropler RJ, Siegel BA, Sampathkumaran K, Pérez JE, Sobel BE, Bergmann SR, Geltman EM. Dependence of recovery of contractile function on maintenance of oxidative metabolism after myocardial infarction. *J Am Coll Cardiol*. 1992;19:989–97.
18. Gropler RJ, Geltman EM, Sampathkumaran K, Pérez JE, Moerlein SM, Sobel BE, et al. Functional recovery after coronary revascularization for chronic coronary artery disease is dependent on maintenance of oxidative metabolism. *J Am Coll Cardiol*. 1992;20:569–77.
19. Schelbert HR. Principles of positron emission tomography. In: Skorton DJ, Schelbert HR, Wolf GL, Brundage BH, editors. *Marcus cardiac imaging: a companion to Braunwald’s heart disease*. 2nd ed. Philadelphia: WB Saunders; 1996. p. 1063–92.
20. Dilsizian V, Bacharach SL, Beanlands SR, Bergmann SR, Delbeke D, Fischman AJ, et al. ASNC imaging guidelines for nuclear cardiology procedures: PET myocardial perfusion and metabolism clinical imaging. *J Nucl Cardiol*. 2009;16:651. <https://doi.org/10.1007/s12350-009-9094-9>.
21. Dilsizian V. Perspectives on the study of human myocardium: viability. In: Dilsizian V, editor. *Myocardial viability: a clinical and scientific treatise*. Armonk: Futura; 2000. p. 3–22.
22. Tillisch J, Brunken R, Marshall R, Schwaiger M, Mandelkern M, Phelps M, Schelbert H. Reversibility of cardiac wall-motion abnormalities predicted by positron tomography. *N Engl J Med*. 1986;314:884–8.
23. Dilsizian V, Arrighi JA. Myocardial viability in chronic coronary artery disease: perfusion, metabolism and contractile reserve. In: Gerson MC, editor. *Cardiac nuclear medicine*. 3rd ed. New York: McGraw-Hill; 1996. p. 143–91.
24. Eitzman D, Al-aouar Z, Kanter HL, vom Dahl J, Kirsh M, Deeb GM, Schwaiger M. Clinical outcome of patients with advanced coronary artery disease after viability studies with positron emission tomography. *J Am Coll Cardiol*. 1992;20:559–65.
25. Di Carli MF, Davidson M, Little R, Khanna S, Mody FV, Brunken RC, et al. Value of metabolic imaging with positron emission tomography for evaluating prognosis in patients with coronary artery disease and left ventricular dysfunction. *Am J Cardiol*. 1994;73:527–33.
26. Di Carli MF, Asgarzadie F, Schelbert HR, Brunken RC, Laks H, Phelps ME, Maddahi J. Quantitative relation between myocardial viability and improvement in heart failure symptoms after revascularization in patients with ischemic cardiomyopathy. *Circulation*. 1995;92:3436–44.
27. Haas F, Haehnel CJ, Picker W, Nekolla S, Martinoff S, Meisner H, Schwaiger M. Preoperative positron emission tomography viability assessment and perioperative and postoperative risk in patients with advanced ischemic heart disease. *J Am Coll Cardiol*. 1997;30:1693–700.
28. Srinivasan G, Kitsiou AN, Bacharach SL, Bartlett ML, Miller-Davis C, Dilsizian V.  $^{18}\text{F}$ -fluorodeoxyglucose single photon emission computed tomography: can it replace PET and thallium SPECT for the assessment of myocardial viability? *Circulation*. 1998;97:843–50.
29. Dilsizian V. FDG uptake as a surrogate marker for antecedent ischemia. *J Nucl Med*. 2008;49:1909–11.
30. Camici P, Araujo LI, Spinks T, Lammertsma AA, Kaski JC, Shea MJ, et al. Increased uptake of 18F-fluorodeoxyglucose in post-ischemic myocardium of patients with exercise-induced angina. *Circulation*. 1986;74:81–8.
31. He ZX, Shi RF, Wu YJ, Tian YQ, Liu XJ, Wang SW, et al. Direct imaging of exercise-induced myocardial ischemia with fluorine-18-labeled deoxyglucose and Tc-99m-sestamibi in coronary artery disease. *Circulation*. 2003;108:1208–13.
32. Dou KF, Yang MF, Yang YJ, Jain D, He ZX. Myocardial 18F-FDG uptake after exercise-induced myocardial ischemia in patients with coronary artery disease. *J Nucl Med*. 2008;49:1986–91.
33. Taegtmeier H, Dilsizian V. Imaging myocardial metabolism and ischemic memory. *Nat Clin Pract Cardiovasc Med*. 2008;5:S42–8.
34. Dilsizian V, Bateman TM, Bergmann SR, Des Prez R, Magram MY, Goodbody AE, et al. Metabolic imaging with beta-methyl-para-[ $^{123}\text{I}$ ]-iodophenyl-pentadecanoic acid (BMIPP) identifies ischemic memory following demand ischemia. *Circulation*. 2005;112:2169–74.



35. Krebs H. The Pasteur effect and the relation between respiration and fermentation. *Essays Biochem.* 1972;8:1–34.
36. Di Carli MF, Prcovski P, Singh TP, Janisse J, Ager J, Muzik O, Vander HR. Myocardial blood flow, function, and metabolism in repetitive stunning. *J Nucl Med.* 2000;41:1227–34.
37. Dickfeld T, Lei P, Dilsizian V, Jeudy J, Dong J, Voudouris A, et al. Integration of three-dimensional scar maps for ventricular tachycardia ablation with positron emission tomography-computed tomography. *JACC Cardiovasc Imaging.* 2008;1:73–82.
38. United States Renal Data System. 2018 USRDS annual data report: Epidemiology of kidney disease in the United States. Bethesda: National Institutes of Health, National Institute of Diabetes and Digestive and Kidney Diseases; 2018.
39. Tyralla K, Amann K. Morphology of the heart and arteries in renal failure. *Kidney Int.* 2003;63:S80–3.
40. Nishimura M, Tsukamoto K, Hasebe N, Tamaki N, Kikuchi K, Ono T. Prediction of cardiac death in hemodialysis patients by myocardial fatty acid imaging. *J Am Coll Cardiol.* 2008;51:139–45.
41. Lodge MA. Evidence for inverse relationship between myocardial glucose utilization with PET and severity of renal dysfunction [abstract]. *J Nucl Med.* 2007;48(Suppl 2):108P.
42. Nishimura M, Hashimoto T, Kobayashi H, Fukuda T, Okino K, Yamamoto N, et al. Myocardial scintigraphy using a fatty acid analogue detects coronary artery disease in hemodialysis patients. *Kidney Int.* 2004;66:811–9.
43. Dilsizian V, Fink J. Deleterious effect of altered myocardial fatty acid metabolism in kidney disease. *J Am Coll Cardiol.* 2008;51:146–8.
44. Fink JC, Lodge MA, Smith MF, Hinduja A, Brown J, Dinits-Pensy MY, Dilsizian V. Pre-clinical myocardial metabolic alterations in chronic kidney disease. *Cardiology.* 2010;116:160–7.
45. Hofmann M, Wollert KC, Meyer GP, Menke A, Arseniev L, Hertenstein B, et al. Monitoring of bone marrow cell homing into the infarcted human myocardium. *Circulation.* 2005;111:2198–202.